DEVELOPMENT OF SELF–SUPPORTED POLYMERIC MEMBRANE FOR CONTAMINANT REMOVAL FROM WASTEWATER

Thesis submitted towards the partial fulfillment of Master of Engineering degree in Chemical Engineering

by

MD IBNE ATA

Class Roll No.: 002210302015

Exam Roll No.: M4CHE24015

Registration No.: 163444 of 2022-2023

Session: 2022 – 2024

Under the guidance of

Dr. Mehabub Rahaman

&

Dr. Saswata Bose

DEPARTMENT OF CHEMICAL ENGINEERING

JADAVPUR UNIVERSITY

Kolkata – 700032

DECLARATION OF ORIGINALITY AND COMPLIANCE OF ACADEMIC ETHICS

I hereby declare that this thesis contains a literature survey and original research work by the undersigned candidate, as part of his "***Master of Engineering in Chemical Engineering***" studies. All information in this document has been obtained and presented in accordance with academic rules and ethical conduct.

I also declare that, as required by these rules and conduct, I have fully cited and referenced all material and results that are not original to the research work.

Name: **MD IBNE ATA**

Registration No.: 163444 of 2022-2023

Thesis Title: **DEVELOPMENT OF SELF–SUPPORTED POLYMERIC COMPOSITE MEMBRANE FOR CONTAMINANT REMOVAL FROM WASTEWATER.**

Signature: Md. Ibne Ata

Date: 14/08/24

CERTIFICATION

This is to certify that **Mr. Md Ibne Ata**, a final year student in the Master of Chemical Engineering examination in the Department of Chemical Engineering, Jadavpur University, bearing Registration No: 145132 has successfully completed the thesis work entitled "**Development Of Self–Supported Polymeric Composite Membrane For Contaminant Removal From Wastewater.**"

"under the guidance of **Dr. Mehabub Rahaman** and **Dr. Saswata Bose** during his master's degree curriculum. This work has not been reported earlier anywhere and can be approved for submission in partial fulfillment of the requirements for the Master of Engineering in Chemical Engineering.

Associate Professor
CHEMICAL ENGINEERING DEPARTMENT
JADAVPUR UNIVERSITY
Kolkata-700 032

Mehabub Rahaman 20.8.24

Dr. Mehabub Rahaman
Supervisor
Chemical Engineering Department
Jadavpur University

Assistant Professor
CHEMICAL ENGINEERING DEPARTMENT
JADAVPUR UNIVERSITY
Kolkata-700 032

16/8/24

Dr. Saswata Bose
Supervisor
Chemical Engineering Department
Jadavpur University

HEAD
CHEMICAL ENGINEERING DEPARTMENT
JADAVPUR UNIVERSITY
Kolkata-700 032

20/8/24

Head of the Department
Chemical Engineering Department
Jadavpur University

Dipak Laha 20/8/24

Dean
Faculty of Engineering & Technology
Jadavpur University

DEAN
Faculty of Engineering & Technology
JADAVPUR UNIVERSITY
KOLKATA-700 032

CERTIFICATE OF APPROVAL

This thesis is hereby approved as the creditable study of an engineering subject carried out and presented in a manner satisfactory to warrant its acceptance as prerequisite to the degree for which it has been submitted. It is understood by this approval that the undersigned don't endorse or approve any statement made, opinion expressed or conclusion drawn therein but approve the thesis only for purpose of which it is submitted.

.....Md. Ibne Ata.....

Md Ibne Ata

Department of Chemical Engineering

Jadavpur University

ACKNOWLEDGEMENT

Though the following project is individual project work, but I would have never been successful in completing my work in a smooth manner without help, guidance, assistance, and inspiration from a lot of people. At the start of this report, I would like to thank all those persons who have helped me in this endeavor. Without their guidance and help it would not be possible for me to progress and plan about this project.

I would sincerely express my gratitude towards my project guide Dr. Mehabub Rahaman, Dr. Saswata Bose, and my senior Mr.Avik Mukherjee (PhD Scholar) for their valuable guidance and cooperation and for providing me the opportunity to accomplish the project. Without their guidance and assistance, I could never work successfully in this area. I am greatly thankful to them for always guiding me throughout my project work.

I would like to thank all my lab mates who consistently helped me while performing and planning this project.

I would also like to express gratitude to the HOD and all faculties and non-teaching staff of the Chemical Engineering Department, Jadavpur University.

Thanking you,
Md Ibne Ata
Class Roll Number – 002210302015
Exam Roll No.: M4CHE24019
Registration Number – 163444 of 2022-2023
M.E. 2nd Year

ABSTRACT

Nanocomposite materials are comprised of metal nanoparticles and graphene oxide (GO) have garnered significant attention across various materials science disciplines due to their vast potential applications. Specifically, the focus of this study was on developing a highly efficient photocatalyst using GO/TiO_2 nanocomposites integrated with metal nanoparticles, which was successfully achieved through a straightforward solvothermal synthesis method. The synthesized nanocomposites underwent thorough characterization employing techniques such as X-ray diffraction (XRD), Fourier transform infrared (FTIR) spectroscopy, scanning electron microscopy (SEM), tensile strength analysis, point of zero charge (PZC) determination, and swelling tests. The membrane fabrication process involved the utilization of N,N Dimethylformamide (DMF), 32wt% polyvinylidene fluoride (PVDF), 16wt% Polyethylene glycol (PEG), and 0.640wt% of the GO/TiO_2 nanocomposite. Subsequently, the photocatalytic performance of these nanocomposites was evaluated through the degradation of various pollutants, namely methylene blue (MB), Safranin O (SO), a mixture of both dyes (SO+MB), and $K_2Cr_2O_7$, a model representative of water pollutants. Remarkably, catalytic degradation efficiencies of 78.388% for MB, 71.52% for SO, 67.638,85.872% for the SO+MB mixture, and 95.09% for $K_2Cr_2O_7$ were achieved when using a nanocomposite containing 7% GO under 120 minutes of UV-A (365 nm) irradiation. Overall, the synthesized nanocomposites demonstrated promising photocatalytic potential, indicating their viability for future environmental remediation applications.

CONTENTS

Declaration of originality and compliance of academic ethics ……. ii

Certification ……. iii

Certificate of approval ……. iv

Acknowledgment …….. v

Abstract ……..…... vi

List of Figures ……...…… ix-x

List of tables ……..……. x

List of abbreviations ……..…… x

Chapter-1(Introduction) ……. 1-14

1.1.Introduction ……. 2-5

1.2.Literature Review ……. 6-14

Chapter-2(Experimental Methodology) …….. 15-24

2.1.Chemicals and Materials ……..…….. 16

2.2. Characterization of GO and GO/TIO2 Composites ……..……. 16

2.3. Membrane Characterization Techniques ……. 17-19

2.4. Synthesis of TIO2- Graphene Oxide Composites ……...……. 20-21

2.5. Preparation of GO/TiO2 Membranes …….…….. 21-22

2.6. Batch Experiment for Photodegradation of MB,SO,Mixed (MB&SO)&K2Cr2O7…..22-23

2.6.1. Calculation Of Photocatalytic Activity …… 22-23

2.7. Degradation Kinetic Study ……...…. 23

2.8. Adsorption Isotherm Model ……..… ….24

Chapter-3(Results and Discussions) ……...……. 25-45

3.1. FTIR Analysis of Nanocomposite ……...…… 26-27

3.2. SEM Analysis of Membrane ……..……... 27-28

3.3. XRD Analysis of Nanocomposite ……..….. 29-30

3.4. PL Analysis of Nanocomposite …….……. 30-31

3.5.Batch Experiment of Membrane ……...…… 31-41

3.5.1.The Point Of Zero Charge ……..…… 31-32

3.5.2. UV-Vis Spectrophotometer Analysis ……..…… 32-34

3.5.3. Photocatalytic Activity ……..…….. 34-38
3.5.4. Degradation kinetics …… 38-39
3.5.5. Adsorption Isotherm Studies ……..……. 40-41
3.6. Tensile Strength Analysis of Membrane ……..…… 41-42
3.7.Swelling Experiment of Membrane ……..….. 43-44
3.8.Regeneration Study of Membrane …… 44-45
Chapter -4(Conclusion) ……..…… 46-47
4.1.Conclusion ……..…… 47
References ……..…… 48-54

LIST OF FIGURES

Figure 1. Basic principles of photodegradation process using semiconductors (example: TiO_2)

Figure 2. GO/TiO_2 was used as an additive to prepare GO/TiO_2–PVDF ultrafiltration membranes, also the grafting PEG worked as a porogen and increased the polarity of the membranes

Figure 3. Using different types of solutions for washing for the Regeneration of membrane

Figure 4. Experimental setup of synthesis of TiO_2- graphene oxide(GO) composites

Figure 5 . Experimental setup of Preparation of GO/TiO_2 membrane/thin film.

Figure 6. Plots of FTIR of nanoparticles and nanocomposites.

Figure 7.SEM image of PVDF-PEG(a,c) and GO/TiO_2-PVDF-PEG(b,d) membrane/thin film
Figure 8. Plots of XRD of nanoparticles and nanocomposites

Figure 9. Plots of PL of nanoparticles and nanocomposites

Figure 10. Plots of determination of the point of zero charge (PZC)

Figure 11a. Plots of the Calibration curve of MB dye

Figure 11b. Plots of the Calibration curve of SO dye

Figure 11C. Plots of the Calibration curve of Mixed dye (MB+SO)

Figure 11d. Plots of the Calibration curve of $K_2Cr_2O_7$.

Figure 12a. Plots of %Removal with time of MB dye in UV-A medium.

Figure 12b. Plots of %Removal with time of SO dye in UV-A medium.

Figure 12c. plots of %Removal with time of Mixed (MB+SO) dye in UV-A medium

12d. Plots of %Removal with time of $K_2Cr_2O_7$ in UV-A medium

Figure 13a.Kinetic plots of the photodegradation reaction of MB and SO dye in the presence of GO/TiO_2 nanocomposites

Figure 13b. Kinetic plots of the photodegradation reaction of Mixed (MB+SO) dye in the presence of GO/TiO_2 nanocomposites

Figure 13c. Kinetic plots of the photodegradation reaction of $K_2Cr_2O_7$ in the presence of GO/TiO_2 nanocomposites.
Figure 14. Isotherm study graphs for Langmuir Isotherm.

Figure 15. Isotherm study graphs for Freundlich isotherm

Figure16. Plots of the Tensile Strength

Figure 17. Plots of %Swelling of the membrane/thin film in different solvents with time

Figure 18 Regeneration of membrane/thin film bar graphs

LIST OF TABLES

Table 1 Isotherm analysis

Table 2. Data of Tensile Strength analysis

LIST OF ABBREVIATIONS

C_2H_5OH = Ethyl Alcohol

DMF = N, N- Dimethylformamide

FTIR = Fourier Transform Infrared Spectroscopy

GO = Graphene Oxide

HCl = Hydrochloric Acid

$K_2Cr_2O_7$ = Potassium Dichromate

MB = Methylene Blue

PEG = Polyethylene glycol

PL = Photoluminescence

PVDF = Polyvinylidene fluoride or polyvinylidene difluoride

PZC = Point of Zero Charge

SEM = Scanning Electron Microscope

SO = Safranin O

TiO_2 = Titanium Dioxide

TS = Tensile Strength

TTIP = Titanium Isopropoxide

UVA = Ultraviolet A

UV-VIS = Ultra Violet-Visible Spectroscopy

XRD = X-ray Diffraction

CHAPTER-1

INTRODUCTION

1.1. INTRODUCTION

Contaminants in water, such as heavy metal ions, pharmaceutical compounds, organic solvents, petroleum products, textile dyes, etc., enter water supplies and the atmosphere from anthropogenic activity and cause environmental and health issues [1]. Membrane technologies have been widely developed for the purification of water over other processes like thermal approaches because does not involve chemical additives and phase changes, also membrane technologies are regarded as cost-effective candidates and play an increasingly important role in the treatment of natural waters and wastewater [2], [3].

Polyvinylidene fluoride (PVDF) is widely used in the preparation of membranes because of its high mechanical strength, chemical stability, good thermal stability[5],[6]. PVDF membranes have the main disadvantage of hydrophobicity can cause severe fouling, which leads to a decrease in the membrane flux and an increase in energy costs during membrane operation[7]. As a result, numerous studies have been carried out by membrane researchers to enhance the hydrophilicity and manage fouling of PVDF membranes. For this objective, the most straightforward and efficient technology devised is membrane hydrophilic modification[8], because it has the ability to enhance the membrane's physicochemical and hydrophilicity, both of which will help to increase the membrane's antifouling qualities[9]. The most often used methods for enhancing membrane hydrophilicity and reducing fouling are the use of hydrophilic polymers or the blending of inorganic nanoparticles with the casting solution[10], [11], [12].

Graphene oxide (GO) is one of the derivatives of graphene, which can be produced through cost-effective chemical functionalization techniques. GO is well-distributed with an abundance of oxygen-containing functional groups such as carboxyl, carboxylic, epoxy and hydroxyl groups. Due to the existence of these oxygenated functional groups, GO possesses high hydrophobicity compared to graphene. Also, GO exhibits a large surface area, excellent chemical stability, and mechanical stability[4] .

Prepared GO/PVDF membrane, which showed better hydrophilicity and antipollution properties. GO can also be modified by an esterification reaction with hydrophilic polyethylene glycol (PEG) to improve its hydrophilicity. It was anticipated that GO would become more hydrophilic when combined with hydrophilic polymers like PEG and that this would also solve

the issue of PEG easily leaking out during membrane development. To improve a PVDF membrane's performance, a significant amount of hydrophilic functional groups—hydroxyl groups—were introduced through the combined action of PEG and GO[13]. Also, a popular and promising strategy has been the functionalization with poly (ethylene glycol) (PEG-GO) through covalent bonding or non-covalent interactions, which imparts remarkably high aqueous stability as well as enhanced biocompatibility[14].

Various semiconductors have been studied extensively for their potential applications as photocatalysts, including widely known materials like titanium (IV) oxide (TiO_2), zinc (II) oxide (ZnO), gallium arsenide, tungsten (VI) oxide (WO_3), gallium phosphide, and cadmium sulfide. These semiconductors have unique properties that make them suitable for use in various photocatalytic reactions, such as water splitting and pollutant degradation. Researchers have been exploring ways to enhance the photocatalytic efficiency of these materials by modifying their surface properties or band structures to improve their performance in photocatalysis.[15]. This process involves charge carrier transfer from the photo-excited semiconductor as shown in Figure 1, which can be summarized into two steps: photoexcitation of the semiconductor, which causes the separation of electrons (e^-) and holes (h^+) as charge carriers, and the migration/recombination of charge carriers with the emission of heat or light. During the first step, when the semiconductor material is exposed to light, electrons are excited to a higher energy state, creating electron-hole pairs. These electron-hole pairs are then free to move within the semiconductor material, leading to the migration of charge carriers. The second step involves the recombination of these charge carriers, where electrons and holes recombine, releasing energy in the form of heat or light [16].Also, TiO_2 has three major crystal structures: rutile, anatase, and brookite [18]. These Crystal structures have different lattice parameters, resulting in different physical and chemical properties. The most commonly used commercial TiO_2 powder is anatase, or a mixture of rutile and anatase, as anatase has the highest photocatalytic activity among all three crystal structures. To obtain a high photocatalytic efficiency, nanoscale materials are often preferred because of their large surface area and high chemical activities. However, the release of nanoparticles in the environment may cause severe genotoxicity and cytotoxicity to aquatic organisms and human beings. It is essential to consider the potential risks associated with the use of nanoscale materials in various applications to ensure the safety of both the environment and human health [19].

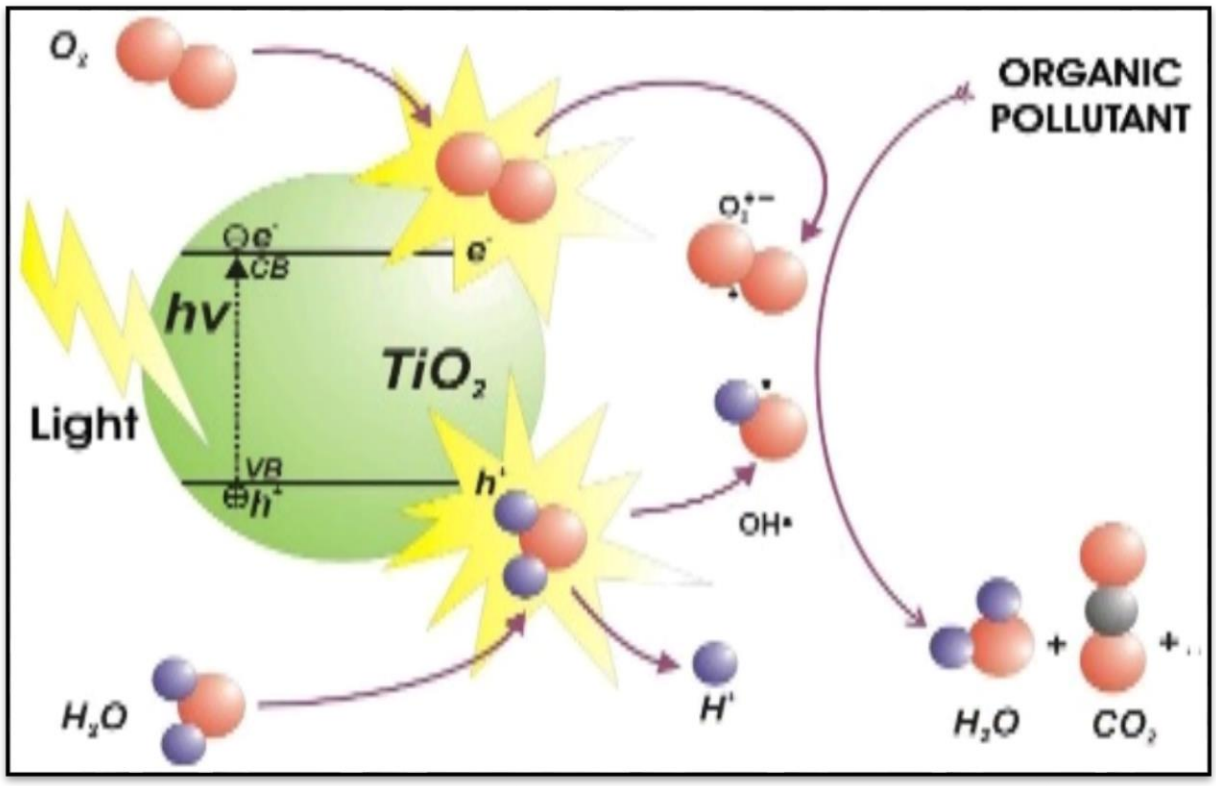


Figure 1. Basic principles of photodegradation process using semiconductors (example: TiO_2)[17].

For a polymeric membrane to be used in a TiO_2/UV process, the membrane has to be stable under UV exposure as well as in an oxidative environment since photocatalysis produces oxidizing diffusing hydroxyl radicals. It is imperative to choose a membrane material that can resist the damaging effects of UV radiation and the reactive nature of hydroxyl radicals to ensure the longevity and efficiency of the membrane in water treatment applications. The ability of the membrane to withstand these harsh conditions is essential for maintaining its separation properties and allowing the photocatalytic process to effectively degrade contaminants in water. By carefully selecting a membrane material that can endure UV exposure and oxidative environments, the TiO_2-activated UV process can achieve optimal performance and deliver clean water for various applications [20]. Based on these considerations, it is crucial to thoroughly investigate the impact of photocatalyzed TiO_2 degradation on polymeric membranes. This research is essential to ensure that the most appropriate membranes are chosen for the photocatalytic reactor process utilizing activated TiO_2. Historically, there have been limited studies conducted on the UV stability of polymeric membranes, mainly due to the minimal demand for membranes that can withstand UV

exposure. Therefore, further exploration in this area is necessary to enhance our understanding of how polymeric membranes react to UV radiation [21].

GO/TiO_2 composite nanomaterials played a crucial role as additives in the development of GO/TiO_2-PVDF hybrid ultrafiltration membranes. The presence of TiO_2 in the PVDF polymeric matrix caused a decrease in both the hydrophilicity and porosity of the membranes. As a result, the water flux and anti-fouling capabilities of the hybrid membranes exhibited an initial increase followed by a subsequent decrease with the rise in TiO_2 content in both TiO_2–GO and PVDF membranes. The introduction of PEG may have been grafted onto GO/TiO_2 functioned as a pore-forming agent during the creation of PVDF membranes, leading to an augmentation of the pore structure on the membrane surface due to the heightened polarity of GO/TiO_2. The incorporation of PEG-modified GO/TiO_2 resulted in a considerable enhancement of the surface hydrophilicity of the PVDF hybrid membranes [22].

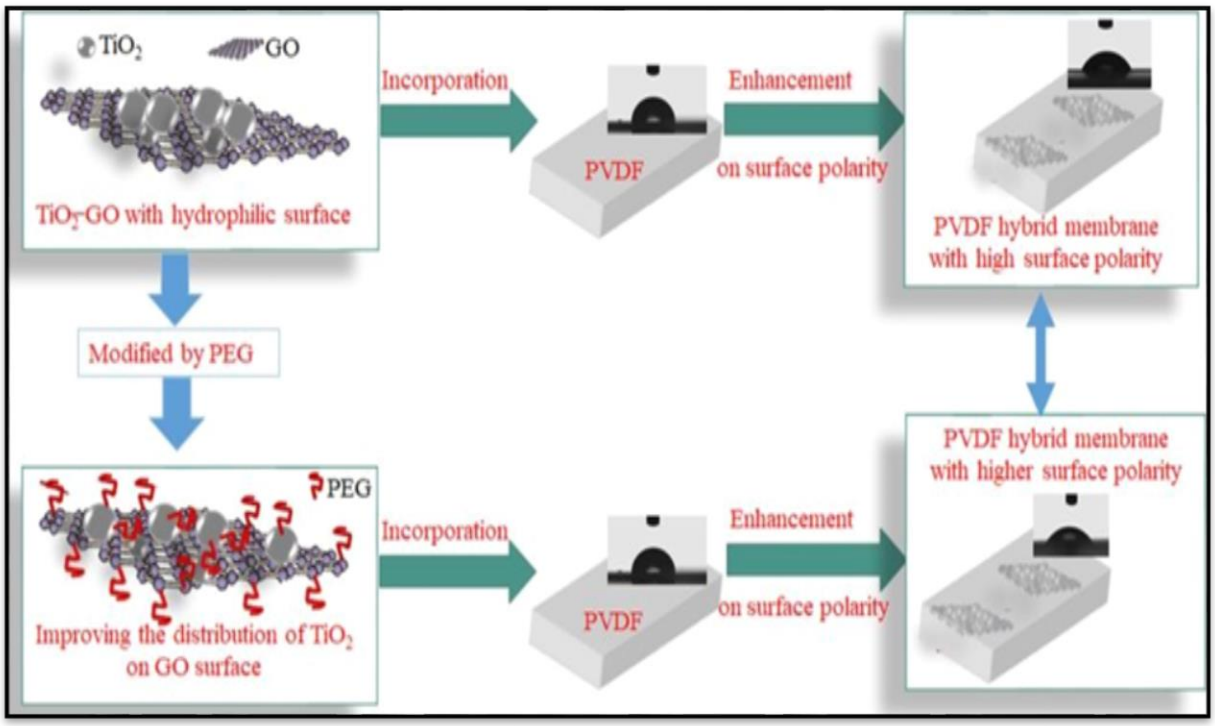


Figure 2. GO/TiO_2 was used as an additive to prepare GO/TiO_2–PVDF ultrafiltration membranes, also the grafting PEG worked as a porogen and increased the polarity of the membranes [22].

1.2. LITERATURE REVIEW

Many researchers have previously worked for preparing GO, GO/TiO_2, GO/TiO_2-PVDF-PEG and the use of adsorption and UV degradation in wastewater treatment. Some of those works are as follows-

Al-Rawashdeh et. al. (2020) Nanocomposite materials based on metal nanoparticles and graphene oxide (GO) have gained increasing attention. In this study, an efficient photocatalyst based on GO/ZnO nanocomposites with embedded metal nanoparticles was successfully synthesized via a simple one-pot method. The photocatalytic activity of the synthesized nanocomposites was tested in the nanocomposite with a percentage of 3.125% GO, after 90 min sunlight irradiation. Nanoparticles were used as dopants to study their effects on the activity of the photocatalyst. This was achieved by the GO−ZnO−Ag nanocomposite. The removal efficiency of MB by the GO−ZnO−Ag nanocomposite was reached. Thus, the GO−ZnO−Ag nanocomposite has the potential to be an efficient adaptable [23].

Dadvar et. al. (2017) Achieving the desired standard of drinking water quality has been one of the concerns across water treatment plants among these methods, unit filtration which employs polymers is one of the new there have been many studies about the use of semiconductive TiO_2 with graphene oxide (GO) on the base of different polymeric membranes for the removal of azo dyes, especially methylene blue (MB). Polymeric GO/TiO_2 membranes investigate the characteristics of different polymeric membranes such as anionic perfluorinated polymer (Nafion), and cellulose acetate, The result of this study showed that the GO/TiO_2 membrane can be used in the field of water treatment and will be used for the removal of polycyclic aromatic hydrocarbons[24].

Prakash (2022) However, recent advancements show promising strategies to improve their photocatalytic activities, including surface modifications using suitable co-catalysts and the development of novel efficient photocatalysts. Graphene oxide (GO) is one of such nanomaterials which shows multifarious roles in photocatalysis with a great potential to act as an independent solar-driven sole photocatalyst. In this minireview, the photochemistry of GO has been discussed in view of its multifarious roles/mechanisms in improving the photocatalytic activity of metal oxide semiconductors, plasmonic nanomaterials, and their nanocomposites [25].

Dai et. al. (2021) A novel reduced graphene oxide/TiO_2-polyphenylenesulfone (rGO/TiO_2-PPSU) hybrid ultrafiltration membrane has been successfully prepared, demonstrating visible-light-driven efficient photocatalytic degradation of organic pollutants. The membrane showed significant improvement in photodegradation towards phenazopyridine hydrochloride solution under ultraviolet and visible light. Its permeability and flux recovery rates showed improved self-cleaning properties under visible light static irradiation, making it a promising candidate for water treatment[26].

Mustafa et. al. (2022) Membrane technology has gained interest for water purification due to the presence of organic micropollutants (EOMPs) in wastewater. Graphene oxide (GO) offers advanced membrane synthesis technologies for EOMP removal due to its superior properties and high oxygen content. Recent advancements in GO membrane synthesis with diverse substrates show improved filtration, adsorption, and degradation efficiencies. GO-assisted water treatment strategies show better permeability, hydrophilicity, and fouling resistance. However, further optimization is needed for the simultaneous removal of multiple contaminants. Future research should focus on determining the GO-assisted OMP removal membrane technology nexus and maximizing its industrial application [27].

Golmohammadi et. al. (2022) The study presents the design and synthesis of Ag-doped BiVO4 nanocomposites embedded in reduced graphene oxide ($BiVO_4$:Ag/rGO) nanocomposites using hydrothermal processing. These photocatalysts showed high efficiency for visible light degradation of model dyes and were used to prepare photocatalytic membranes using polyvinylidene fluoride (PVDF) or polyethylene glycol (PEG)-modified polyimide (PI)[28].

Romão et. al. (2014) A novel high throughput photocatalyst efficiency assessment method is presented using 96-well microplates and UV-vis spectroscopy. The method's reproducibility is demonstrated using methyl orange decomposition and kinetic data are compared with existing literature [29].

Thiruvenkatachari et. al. (2008) Advanced oxidation processes using UV irradiation and photocatalyst titanium dioxide (TiO_2) are increasingly being used for wastewater treatment. This process is effective for treating organic contaminants and persistent organic pollutants. TiO_2 is commonly used in a titanium dioxide-suspended slurry reactor due to its efficiency. However, this

system requires TiO_2 separation from water. A membrane hybrid system, involving coagulation, sedimentation, and microfiltration, has been found to effectively remove TiO_2 and reuse it for a photocatalytic process [30].

Rosu et. al. (2017) The study investigated the photocatalytic degradation of azo dyes using TiO_2-Pt nanoparticles, TiO_2-Pt/graphene oxide, and TiO2-Pt/reduced graphene oxide composites in UV and natural sunlight. The composites showed high efficiency under sunlight conditions, with TPt-GO nanocomposite showing higher photoactivity. The degradation process follows a pseudo-first-order kinetic and a direct dependence between the degradation rate and the chemical structure of the dyes [31].

Zhang et. al. (2014) This study investigates the efficiency of ZnO-based photocatalysts by introducing graphene oxide (GO) and Pd nanoparticles. The results show that when the ZnO-GO ratio is 0.85:0.15, the as-synthesized ZnO−GO nanocomposite shows maximum efficiency on methylene blue, almost 10 times faster than pure ZnO under UV illumination. The combination of GO and Pd nanoparticles is expected to have broad environmental conservation applications [32].

Soltani et. al. (2013) Ferrite bismuth nanoparticles were synthesized via ultrasound as visible light photocatalysts. They were used to degrade methylene blue, a dye pollutant. The degradation efficiency and chemical oxygen demand reduction were 100% and 83%, respectively, under different conditions. Optimum conditions were found for the sono-synthesis of the catalyst [33].

Prakash et. al. (2018) Plasmonic photocatalyst nanomaterials are emerging as novel materials for advanced engineering applications. This review article provides a comprehensive overview of the interdisciplinary aspects of these nanocomposites and their multidisciplinary applications in various fields, including energy, environment, and biomedical. The combination of TiO_2 photocatalyst with noble metal nanostructures shows potential for multidisciplinary applications due to high solar energy utilization. These nanocomposites also exhibit enhanced transport properties and visible light activity due to Schottky and plasmonic effects. They can also be used as surface-enhanced Raman scattering substrates for ultra-detection of bio-organic molecules [34].

Singh et. al. (2017) This mini-review discusses recent developments in designing high-performance photocatalytic systems using functional nanomaterials like graphene, noble metals, and metal oxide nanostructures. The focus is on improving optical properties, charge separations, high charge transfer, and efficiency. Functionalization of metal oxide photocatalysts with noble metals and graphene nanostructures has gained interest in developing these systems. These multicomponent nanocomposite systems offer improved optoelectronic properties due to their excellent electronic and surface plasmon resonance properties [35].

Singh et. al. (2017) This study present the development of dual functional TiO_2 nanofibers (TNF) with different tantalum doping (1-10 mol%) using a simple electrospinning technique. The TNFs show a mesoporous dominant structure, favorable for photocatalytic activity due to catalytic spots. Ta doping decreases the crystalline size and enhances visible light absorption. The optimal 5% Ta-doped TNF showed 5.1 and 2.2 times higher photocatalytic activity under UV and solar light irradiation, respectively. The enhanced photocatalytic and SERS activities can be attributed to enhanced visible light absorption, lower crystalline size, and slightly higher surface area[36].

Kumar et. al. (2016) This study synthesizes graphene oxide (GO) nanosheets (NSs) with precise control over the thickness and molecular structure. Oxygen-containing functional groups on GO NSs provide remarkable optical properties. Various techniques were used to confirm the phase, degree of oxidation, morphology, structural formation, and chemical structure. UV Vis spectroscopy was used to study optical absorption properties. The luminescence peak position can be easily tuned. The synthesized GO NSs can be used as sunlight-active photocatalysts, validating their potential in solar energy conversion [37].

Govindan et. al. (2019) This study discusses the photocatalytic mechanism and performance of carbocatalyst GO in the presence of an electron scavenger (ES). The single-layer GO nanosheet was synthesized using Hummer's method, and the photocatalyst characteristics were gathered through various analytical methods. The study found that GO achieved 24% mineralization efficiency in the absence of ES, while in the presence of ES, it increased to 91%, 77%, and 65% [38].

Gupta et. al. (2021) Titanium dioxide (TiO_2) is a highly effective semiconductor photocatalyst with an optical band gap of 3.2 eV. Its optical band gap and photocatalytic properties

can be improved by tailoring its shape, size, composition, and morphology. Hydrothermal synthesis methods have been used to produce nanostructured TiO_2 materials with improved optoelectronic properties. One-dimensional TiO_2 nanorods (NRs) are particularly important due to their dense structure, quantum confinement effect, high aspect ratio, and large specific surface area. Recent developments in NR synthesis and surface modification strategies have improved their photocatalytic activities [39].

Víctor-Román et. al. (2020) This study investigates the influence of graphene oxide (GO) surface chemistry on the photocatalytic degradation of methylene blue. Benchmark ZnO-GO hybrid materials were synthesized using microwave synthesis and GO with different oxidation degrees. Structural and physical-chemical characterizations show GO's surface chemistry enhances catalytic activity by establishing photo-induced charge-transfer interface interactions with ZnO. The optimized interface interactions resulted in a ZnO-GO catalyst with an 80% conversion rate [40].

Nguyen-Phan et. al. (2011) Titanium dioxide/graphene oxide composites showed superior adsorption and photocatalysis performance under UV and visible radiation. Gradually increasing graphene oxide content up to 10% increased removal efficiency and facilitated methylene blue photodegradation. This was due to synergy effects, increased specific surface area, and ionic interactions between dye molecules and aromatic rings [41].

Iqbal et. al. (2017) study demonstrates the fabrication of a mesoporous TiO_2–rGO nanocomposite using titanic sulfate as the TiO_2 source. The composites were characterized using transmission electron microscopy, X-ray diffraction, UV–Vis diffuse reflectance spectra, and photoluminescence spectra. The nanocomposites showed high photocatalytic activity in the photodegradation of rhodamine B and phenol due to their mesoporous structure [42].

Haldorai et. al. (2014) A supercritical route was used to decorate silver nanoparticles (Ag NPs) on graphene oxide (GO) using glucose as a reducing agent. The resulting Ag/GO nanocomposite was highly efficient in degrading Rhodamine 123 dye and acetaldehyde under visible-light irradiation, with enhanced adsorption and separation efficiency. The nanocomposite also showed excellent antibacterial activity against gram-positive and gram-negative microorganisms [43].

Krishnamoorthy et. al. (2011) The study investigated the photocatalytic properties of graphene oxide nanostructures synthesized using a modified Hummer's method. The results showed excellent photocatalytic activity, reducing resazurin into resorufin in UV irradiation, with pseudo-first-order reaction kinetics, indicating GO's potential as a photocatalyst [44].

Singh et. al. (2018) Graphene oxide (GO) is a biocompatible material that can be easily mixed with ceramic or polymer matrixes. This study investigates its photocatalytic and antibacterial activities. GO nanosheets with excellent morphology exhibit efficient photocatalytic activity towards Congo red dye, demonstrating new possibilities for the degradation of toxic organic pollutants. The study also evaluates the effect of GO dose and its antibacterial activity by growing Escherichia coli and Bacillus on LB agar plates [45].

Chen et al. (2021) Aminated graphene oxide (NGO) was synthesized by combining graphene oxide and diethylenetriamine. The NGO-TiO_2 composite catalysts were self-assembled using a two-phase system. The performance of the composite catalysts was evaluated using methyl orange dye degradation. The NGO-TiO_2 catalyst outperformed TiO_2 and GO-TiO_2 with increasing NGO loading. The introduction of NGO improves TiO_2 catalytic performance and addresses pollution posttreatment issues [46].

Gao et. al. (2014) study uses graphene oxide (GO) nanomaterials to enhance the photocatalytic activities of water filtration membranes. The researchers used a layer-by-layer approach to deposit TiO_2 nanoparticles and GO nanosheets on a polysulfone base membrane. The modified membranes showed significantly faster methylene blue photodegradation kinetics under UV and sunlight, and increased membrane flux due to improved hydrophilicity and contaminant degradation [47].

Riegel et. al. (1995) study investigates the pre-steady-state photoproduction of hydroxyl radicals (OH) from TiO_2 samples using spin trapping and EPR spectroscopy. The efficiency variations, particularly for anatase and rutile crystal forms of TiO_2, are found under pre-steady-state conditions. Variations in the rate constants related to recombination and/or oxidation cause the observed variability in steady-state photocatalytic efficiency [48].

Hunge et. al. (2020) The current research work deals with the preparation of TiO_2 and GO/TiO_2 composite by simple, chemical, cost-effective hydrothermal method. Graphene oxide

(GO) is prepared by modified Hummer's method. Dispersion of GO is achieved by an ultrasonic cleaning bath for 1h. using a power of 200 W and at a frequency of 40 kHz. The prepared catalyst material is characterized by different characterization techniques. XRD study confirms the prepared material is polycrystalline in nature. The synthesized TiO_2 and GO/TiO_2 photocatalyst materials are used to study the photocatalytic degradation of salicylic acid under sunlight illumination. GO/TiO_2 composite shows superior photocatalytic activity than TiO_2. GO/TiO_2 composite shows 57 % degradation of salicylic acid. Mineralization of salicylic acid is studied using chemical oxygen demand [49].

Nguyen et. al. (2020) study examines the fabrication of nanostructured TiO_2/ZnO/reduced graphene oxide (TZR) composites using a simple hydrothermal process. The composites were tested for their photocatalytic performance on methylene blue, rhodamine B, and methyl orange under UV/simulated solar illumination. The synergism of TZR composites showed greater activity, with the highest degradation and mineralization achieved [50].

Romay et. al. (2020) Photocatalytic membrane reactors (PMR) are crucial for process intensification and clean water production. However, successful synthesis faces challenges like reduced photocatalytic activity, photocatalyst stability, and membrane aging. This review critically analyzes these limitations and establishes guidelines to improve the performance of polymeric photocatalytic membranes. It focuses on factors affecting membrane aging and stability, aiming to enhance technological competitiveness in suspended photocatalytic systems [51].

Tran et. al. (2020) The study investigated the efficiency of photocatalytic PVDF-TiO_2 composite membranes under UV irradiation. The membrane surface becomes more hydrophilic, leading to a gradual increase in permeating flux during photo-filtration. The study also investigates the role of UV irradiation mode on flux behavior during photo-filtration. It found that effective flux recovery occurs under UV irradiances equal to or higher than a threshold value, suggesting that photo-filtration can be performed efficiently yet economically [52].

Chang et. al. (2014) This study investigates the effects of asymmetric PVDF composite ultrafiltration membranes containing graphene oxides (GO) and polyvinylpyrrolidone (PVP) on membrane surface compositions, morphology, and performance. The study uses X-ray photoelectron spectroscopy, FTIR-ATR, atomic force microscopy, scanning electron microscopy,

and contact angle to analyze the chemical properties, surface hydrophilicity, and anti-fouling performance of the membranes. The optimized performance was achieved when PVP content was 0.25 wt.% and GO content was 0.5 wt.% [53].

Bhatia et. al. (2021) A four-factor three-level Box-Behnken design (BBD) was used to analyze the photocatalytic degradation of atenolol in an aqueous solution in slurry mode. The model considered factors like catalyst dose, pH, atenolol concentration, and light intensity. The optimum degradation rate was predicted at 0.845 min 1, with substrate concentration and light intensity having the highest positive effects. The GO/ZnO composite showed a faster rate of degradation compared to the Graphene/TiO_2 composite [54].

Ajmal et. al. (2014) Synthetic dye production exceeds 7-10 tons annually, with around 1,000 tons of non-biodegradable textile dyes discharged into natural streams and water bodies. Environmental concerns demand cost-effective dye removal technologies. Advanced oxidation processes using semiconductor nanoparticles are considered an efficient solution. TiO_2, with its high potential for photocatalysis, has gained interest due to its ability to degrade various organic materials, including dyes. Recent advancements include doping with metals, structural modifications, and immobilization for flexible and cost-effective commercial dye treatment [55].

Cigdem (2012) This study explores the use of activated carbon for removing Methylene Blue from wastewater using reaction-based and diffusion-based models. Results show that activated carbon has a high potential as an effective adsorbent for methylene blue adsorption, with the pseudo-second-order equation being the best model, with approximately 99% of activated carbon regenerated through desorption [56].

Kangralkar et. al. (2021) Cuprous oxide nanoparticles (Cu_2O) were prepared using $Cu(NO_3)_2$ and T. arjuna bark extract under microwave irradiation. They were used for removing hexavalent chromium and different dyes through adsorption and photodegradation. The maximum adsorption occurred at pH 8. Photocatalytic degradation of rhodamine b, rose bengal, and methyl red was more effective, but the final products are not safe [57].

Mousa et. al. (2023) The study developed a graphene oxide (GO) membrane with improved photocatalytic properties by incorporating tin dioxide (SnO_2) and titanium dioxide (TiO_2) nanoparticles into a polyvinyl chloride (PVC) matrix. The addition of NPs increased the

porosity of the membrane surface, resulting in increased water flux and removal efficiency. The GO/SnO_2 nanocomposites membrane showed the highest photocatalytic degradation up to a rejection rate of 98% compared to an unmodified membrane [58].

Bunkin et. al. (2021) Photoluminescence spectroscopy experiments examined the interaction mode of the Nafion polymer membrane with amino acids. The study focused on the unwinding effect of polymer fibers in ordinary water and deuterium-depleted water. The interaction with the membrane surface led to the quenching of luminescence from luminescence centers. The study observed dynamic regimes, including triggering effects, similar to computer logical gates [59].

Zheng et. al. (2009) The development of an ultrafiltration technique using a polyethersulfone membrane has led to the adsorption and recovery of methylene blue (MB) from aqueous solutions. The process, which can reach a 100% rejection ratio, can be effectively used in wastewater treatment by reducing the solution pH[60].

CHAPTER-2

EXPERIMENTAL METHODOLOGY

2.1. CHEMICALS AND MATERIALS

Graphene Oxide (GO) was purchased from Platonic Nanotech Private Limited. N, N-Dimethyl formamide (DMF), Polyethylene Glycol 600 (PEG), 2-Propanol, Acetic Acid Glacial and Hydrochloric Acid 37 were purchased from Merck Life Science Private Limited. (Poly) Vinylidene Fluoride (PVDF) was purchased from Thermo Fisher Scientific India Private Ltd. Titanium (IV) Isopropoxide (TTIP) was purchased from Sigma-Aldrich Chemicals Pvt Ltd. Ethanol, absolute was purchased from Changshu Hongsheng Fine Chemical Co.Ltd.UV-A(TL 18W BLB, wavelength 365nm).

2.2. CHARACTERIZATION OF GO AND GO/TIO_2 COMPOSITES

The characterization of the adsorbent was meticulously conducted through a series of comprehensive analytical techniques. Initially, an X-ray diffraction study, facilitating the identification of crystalline phases present within the adsorbent. Furthermore, **PL** has also been used in in situ experiments to characterize interfaces. PL spectroscopy has, for example, been applied to understand the surface processes in the field of semiconductor photocatalysis. The technique provides important information on the optical and photochemical properties of semiconductors, electronic structure of the materials, and also point defects in the interfacial region. To prepare the raw material and adsorbent for further experimentation, a Spac-N-Service Hot Air Oven with a maximum temperature of 300°C and power rating of 1.5 kW was utilized for efficient drying. Subsequently, the heating process was meticulously executed in a Spac-N-Service Muffle Furnace, capable of reaching temperatures up to 1000°C with a power output of 4 kW. The utilization of such precise equipment ensured the preservation of material integrity while undergoing thermal treatments.During the stirring processes crucial for various experiments, a reliable and efficient Remi 2MLH magnetic stirrer was employed to facilitate homogenous mixing and ensure consistent reaction conditions. Moreover, to accurately monitor and adjust the pH of solutions involved in the study, the sophisticated Eutech PC 2700 pH meter was utilized, enabling precise control over reaction parameters and ensuring the reproducibility of results across experiments.

2.3. MEMBRANE CHARACTERIZATION TECHNIQUES

The optical properties of hybrid membranes were investigated by using ultraviolet-visible diffuse reflection spectroscopy (UV-Vis DRS; PerkinElmer Instrument, 1901 Lambda 950). The top surface and cross-section morphology of hybrid membranes were investigated by SEM after fracturing in liquid nitrogen and gold spraying.

The spectrophotometric analysis was conducted using a Perkin-Elmer Lambda 365 UV-Vis Spectrophotometer to examine the compounds MB, SO, a mixture of MB and SO, and $K_2Cr_2O_7$. Specifically, the peak wavelengths detected during the analysis process were pinpointed at 664 nm for MB, 521 nm for SO, and 350 nm for $K_2Cr_2O_7$. To achieve precise measurements, the spectrophotometer was programmed with a scanning interval of 0.5 nm, and the speed of the scan was set at 200 nm per minute to ensure meticulous data collection.

The point of zero charge process, also known as the pHpzc process, is a critical method utilized in the production of graphene oxide membrane/thin film to prevent any unintended release of graphene oxide into the environment. This process is essential for maintaining environmental safety standards during the entire lifecycle of these membrane/thin films, including their production, usage, and disposal. Graphene oxide, a versatile material with promising applications in diverse fields such as electronics, energy storage, and biomedicine, necessitates careful handling to avoid any negative impact on the environment.To determine the pHpzc of the GO/TiO_2 membrane/thin film sample, a traditional batch equilibrium method was employed. This method involved the preparation of five 50 mL solutions in 100 mL Erlenmeyer flasks, with each flask initially adjusted to a specific pH (pHi= 2, 4, 6, 8, 10). Subsequently, 4cm2 (equivalent to 0.0615gm) of GO/TiO_2 membrane was introduced into each solution, and the suspensions were agitated for 24 hours at room temperature (30 ◦C) to achieve equilibrium pH levels. Following this, the final pH (pHf) was measured using a pH meter, and the difference between pHf and pHi was calculated and plotted against pHi to analyze the behavior of the GO/TiO_2 membrane/thin film under different pH conditions.

Measuring the **swelling** of a polymer membrane in the laboratory involves understanding how the membrane responds to solvents. Here are some methods that can be used: the Gravimetric Method and small-angle Xray Scattering (SAXS), in this study we used the **Gravimetric Method** because for bulk swelling gravimetric measurements are more efficient and easy. Measure the dry weight or volume of the polymer membrane/thin film before swelling. Immerse the membrane/thin film

in a solvent until it reaches equilibrium swelling. Measure the weight or volume of the swollen membrane/thin film after equilibrium. Calculate the degree of swelling using the following ratio:

$$Percentage\ of\ Swelling(G) = \frac{m-m_0}{m_0} * 100 \ldots\ldots\ldots\ldots\ldots\ldots\ldots\ldots\ldots\ldots(1)$$

where: (m) is the mass of the wet membrane/thin film.

(m_0) is the mass of the dry membrane/thin film.

Tensile strength, which refers to the maximum stress a material can withstand before breaking under tension, plays a pivotal role in the assessment of polymeric membranes. Researchers and engineers heavily rely on measuring tensile strength to evaluate the robustness and mechanical durability of these membranes, ensuring they can endure the demanding application scenarios they are designed for, including filtration, separation, and structural support. By comprehending the tensile strength characteristics of a membrane, material selection, and design decisions are guided, tailoring the choice of polymers and thickness to enhance operational longevity and prevent premature failure. For instance, when innovating a membrane solution for water treatment purposes, the knowledge of its tensile strength parameters empowers the selection of suitable materials that can withstand the harsh operational conditions inherent in water treatment processes. Moreover, in the course of membrane fabrication, manufacturers can proactively track and assess tensile strength values to guarantee a consistent level of quality in the end product. Any deviations from the expected tensile strength benchmarks may indicate potential process irregularities or material defects, prompting necessary adjustments to uphold the expected quality standards and performance reliability of the membranes. In essence, the intricate interplay between tensile strength evaluation and material engineering not only influences the efficacy and durability of polymeric membranes but also underpins the entire manufacturing process, ensuring optimal performance outcomes and longevity in a variety of industrial applications.

Polymeric membranes, known for their extensive use across diverse industrial sectors, inevitably undergo deterioration over time due to various factors such as fouling, mechanical wear, or chemical damage. **Regeneration** of these membranes becomes a critical task for several compelling reasons. Firstly, fouling mitigation stands out as a primary objective during the regeneration process. Over time, membranes tend to accumulate deposits that impede water permeation, thus necessitating regeneration to reinstate their original efficiency. This restoration not only aids in reducing trans-membrane pressure but also contributes to substantial energy savings. Moreover, sustainability emerges as a key driver behind the need for membrane

regeneration. By recycling membranes through the regeneration process, the generation of waste is minimized, thereby curbing the overall environmental impact. Emphasizing proper disposal methods and adherence to replacement protocols remains crucial to upholding environmental stewardship. Furthermore, cost efficiency remains a paramount consideration in the decision to regenerate membranes. Extending the lifespan of membranes through regeneration translates to tangible cost savings that would otherwise be incurred by frequent replacements. This cost-effective approach not only optimizes resources but also ensures the sustained functionality of membranes within industrial operations. In essence, the regeneration of polymeric membranes stands as a multifaceted solution encompassing efficacy, sustainability, and economic benefits for various industrial applications. In this study, various desorption solutions were utilized for membrane regeneration, including pure hydrochloric acid (HCl), pure ethanol, a combination of equal parts HCl and ethanol, a mixture of equal volumes of sodium hydroxide (NaOH) and ethanol, and a blend of equal volumes of acetic acid and ethanol. Notably, it was found that a blend of HCl and ethanol in equal proportions yielded superior results and was deemed more optimal for the regeneration process. The utilization of different solutions served to explore the effectiveness of each combination in restoring membrane/thin film function and enhancing performance. By analyzing the outcomes of employing these different solvents, valuable insights were gained



50%HCl +50%C_2H_2OH	100%C_2H_2OH	100%HCl	50%Acetic acid+ 50%C_2H_5OH	50%NaOH+ 50%C_2H_5OH

Figure 3. Using different types of solutions for washing for the Regeneration of membrane

into the most effective approach for achieving successful membrane regeneration. Additionally, the study aimed to elucidate the impact of varying desorption solutions on the overall efficacy of the regeneration process. Integrating different solvent combinations allowed for a comprehensive assessment of the most suitable option for achieving optimal membrane regeneration. Ultimately, the preference for the mixture of equal parts HCl and ethanol indicates the potential for this specific solution to serve as a preferred method for enhancing membrane performance through effective regeneration techniques.

2.4. SYNTHESIS OF TIO_2- GRAPHENE OXIDE COMPOSITES

To synthesize TiO_2-GO composites via the solvothermal method, a specific procedure was followed. Initially, a mixture comprising 70 mL of 2-Propanol and 5 mL of acetic acid was prepared in a 250 mL round-bottomed flask, containing 7 wt% of GO, which was vigorously stirred for up to 5 minutes to ensure thorough blending. Subsequently, the dispersion of GO within the reaction mixture was achieved through sonication for a period of 30 minutes. Upon attainment of homogeneous dispersion, 10 mL of TTIP was introduced into the well-blended GO solution and stirred vigorously for an extended duration of 2 hours. The resulting reaction mix was then

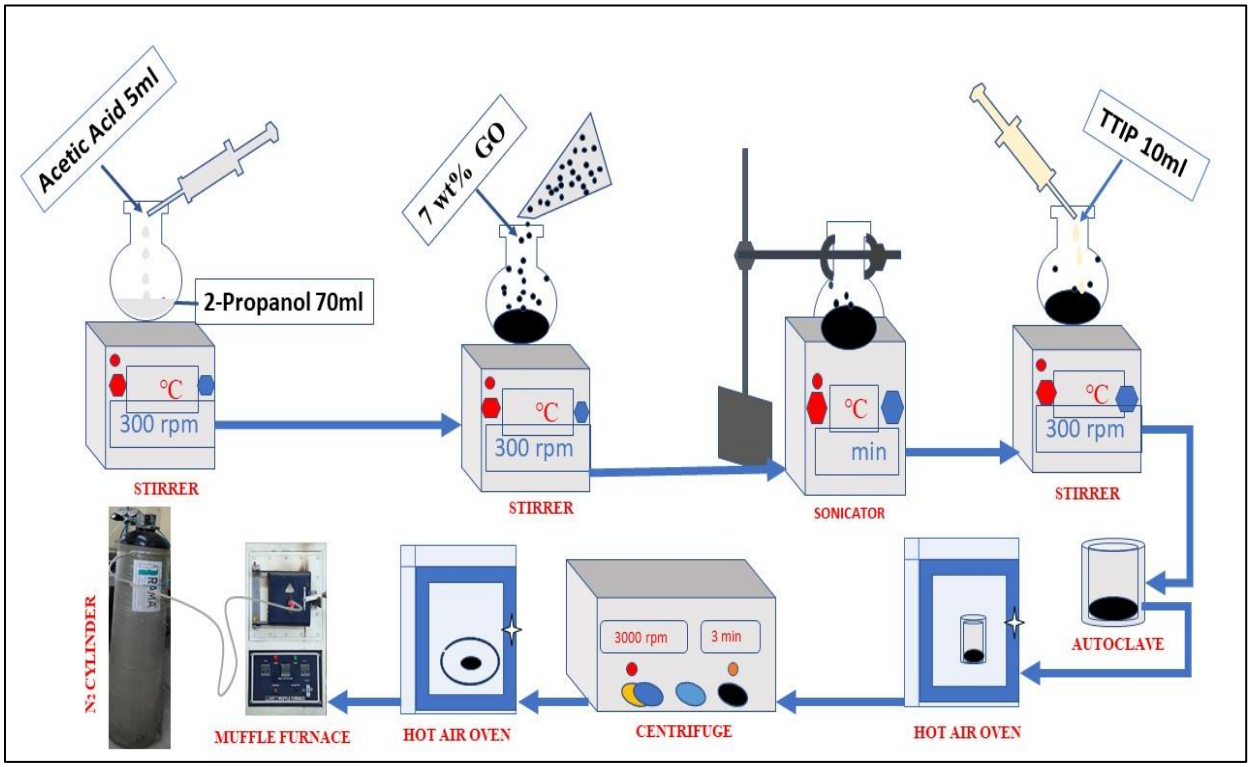


Figure 4. Experimental setup of synthesis of TiO_2- graphene oxide(GO) composites.

carefully transferred into a Teflon-lined autoclave reactor and subjected to heating in a hot air oven at a controlled temperature of 120 °C for a duration of 24 hours. Following the completion of this heating process, the autoclave was permitted to cool down to room temperature gradually. The ensuing product was carefully separated by means of centrifugation and subsequently washed repeatedly with both deionized water and ethanol to ensure purification. Finally, the ultimate product was subjected to drying at a temperature of 70 °C for a total duration of 12 hours to facilitate the complete evaporation of the solvent content. This prepared TiO_2/GO composite was

thereafter subjected to an annealing process at a higher temperature of 500 °C for an extended period of 3 hours, maintaining a specific ramping rate of 2 °C min^{-1} under a controlled nitrogen atmosphere within a specialized muffle furnace system for optimal results to be achieved during the structural transformation.

2.5. Preparation of GO/TiO_2 Membranes/Thin Film

The synthesis procedure involved the utilization of a total volume of 20 ml of dimethylformamide (DMF). In the initial step, 10 ml of DMF was carefully introduced into a volumetric flask. Subsequently, polyvinylidene fluoride (PVDF) was added in an amount corresponding to 32% of the DMF used. Following this, a calculated proportion of 0.5 of the PVDF quantity was supplemented by the addition of polyethylene glycol (PEG). Incorporation of titanium dioxide-graphene oxide (TiO_2-GO) was then carried out, with the amount equivalent to 2% of the PVDF volume. Throughout these processes, a consistent temperature of 60°C was maintained within a water bath, with continuous stirring conducted over a duration of 12 hours.

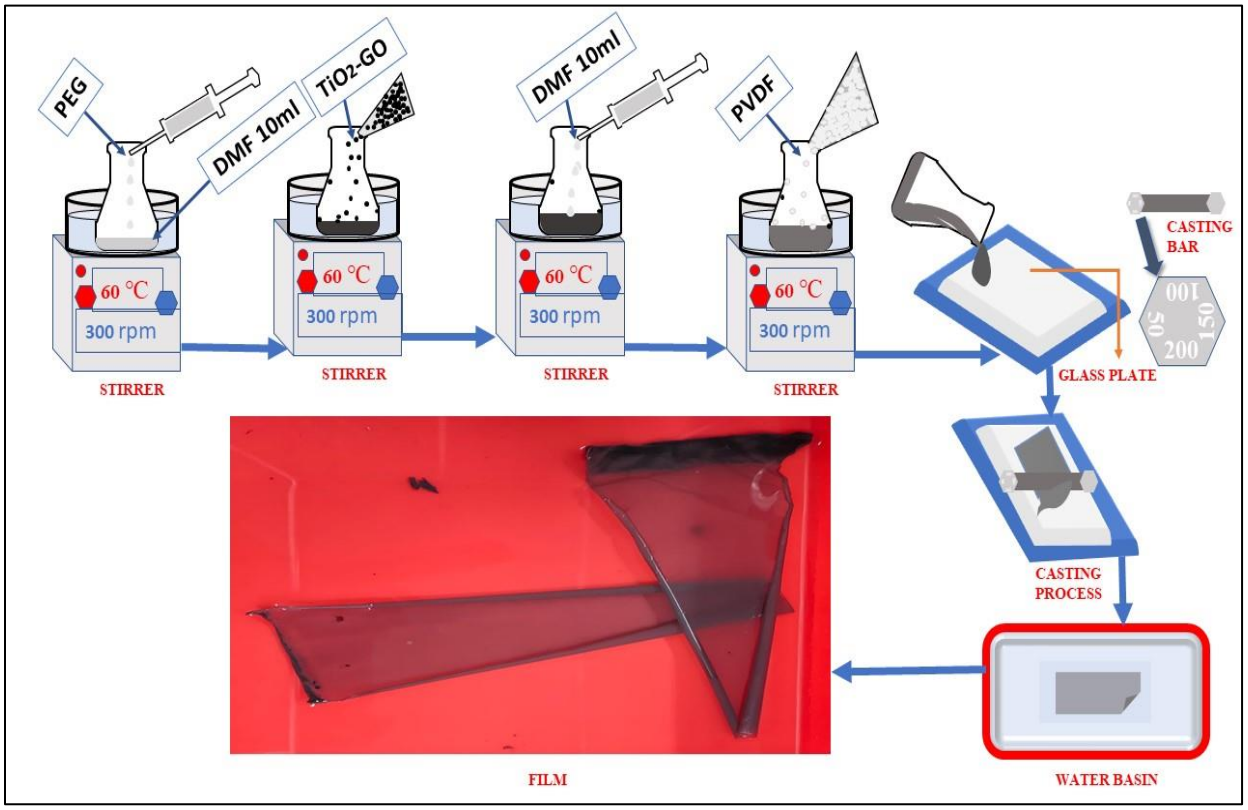


Figure 5 . Experimental setup of Preparation of GO/TiO_2 membrane/thin film.

The remaining 10 ml of DMF was subsequently introduced into the existing solution, in addition to a gradual introduction of the PVDF component. This continuation of the procedure also took place within a water bath environment at 60°C, with stirring maintained for an additional 12 hours. Once the preparation was deemed complete, the solution was deemed suitable for casting, utilizing a casting bar and glass plate for the process. Post-casting, the glass plate was carefully submerged in a water basin, facilitating the automatic detachment of the produced film from the glass surface. This systematic approach ensured the successful fabrication of the desired film composite. In a single batch of reaction of volume 20ml, about 625cm^2 of membrane could be casted on an average.

2.6. BATCH EXPERIMENT FOR PHOTODEGRADATION OF MB, SO, MIXED (MB & SO) AND $K_2Cr_2O_7$

A series of standard solutions were prepared for MB and SO with varying concentrations ranging from 5 mg/L to 20 mg/L for MB and 5 mg/L to 25 mg/L for SO. Additionally, mixed solutions containing both MB and SO were also prepared with concentrations from 5 mg/L to 30 mg/L. Furthermore, $K_2Cr_2O_7$ solutions were prepared with concentrations ranging from 5 mg/L to 30 mg/L for calibration purposes using UV-Vis Spectroscopy to establish the relationship between absorbance and concentration. By analyzing the calibration curve derived from these solutions, a clear correlation between absorbance and concentration was determined. These calibration results are extensively detailed in Chapter 3 of the study.

2.6.1. Calculation Of Photocatalytic Activity

The first step involves exposing the one-hour film sample to a dark medium to facilitate adsorption. Subsequently, the sample is transitioned into a UV medium where it undergoes UV degradation. This sequence of processes allows for the effective examination and study of the film's characteristics under different environmental conditions. The initial placement in the dark medium serves to prepare the sample for further experimentation by enhancing its interaction with external factors. Upon transfer to the UV medium, the degradation process initiates, serving as a crucial phase in evaluating the film's resilience and properties when subjected to ultraviolet light exposure. Overall, this methodical approach ensures a comprehensive assessment of the film's behavior and performance in varying settings, enabling researchers to draw meaningful

conclusions regarding its stability and potential applications. The total percentages of adsorption were evaluated using Equation 2

$$Adsorption\ efficency(\%) = \frac{C_i - C_0}{C_i} * 100 \quad \text{.....(2)}$$

where C_i represents the initial concentration of dye and C_0 is the concentration of dye after adsorption.

The total percentages of photodegradation were evaluated using Equation 3

$$Photocatalytic\ efficency(\%) = \frac{C_0 - C}{C_0} * 100 \quad \text{.....(3)}$$

where C_0 represents the after-adsorption concentration of dye and C is the concentration of dye after degradation.

2.7. DEGRADATION KINETIC STUDY

The photodegradation reactions for dye follow pseudo-first-order kinetics, By analyzing the rate of dye degradation over time, we can estimate the precise values of these rate constants, which play a crucial role in understanding the degradation process. The pseudo-first-order kinetics model provides valuable insights into the mechanism and efficiency of the catalytic reactions during UV irradiation, shedding light on how the dye molecules break down under specific conditions. Overall, this approach allows us to quantitatively assess the degradation kinetics and better grasp the intricate interplay between the dye molecules and the UV light, ultimately advancing our knowledge in this area of study [61].

$$Ln\left(\frac{C}{C_0}\right) = -kt \quad \text{.....(4)}$$

Where:

C_0 is the initial concentration.

C is the final concentration after degradation.

t is the degradation time

k is the degradation rate constant.

2.8. ADSORPTION ISOTHERM MODEL

Adsorption capacity, the following equations were used-

$$Adsorption\ capacity = q_e\left(\frac{mg}{g}\right) = (C_0 - C_e)\frac{V}{m} \quad \text{.....(5)}$$

Where C_0 is the initial dye concentration, C is the dye concentration at t min, C_e is the dye concentration at equilibrium, V is the volume of the wastewater in mL and m is the mass of the added adsorbent in mg.

Langmuir and Freundlich's isotherm was applied for analyzing adsorption isotherm data. The mathematical equation for Langmuir isotherm is expressed as follows:

$$q_e = \frac{Q_{max}K_LC_e}{(1+K_LC_e)} \text{ or } \frac{1}{q_e} = \frac{1}{K_LQ_{max}}\frac{1}{C_e} + \frac{1}{Q_{max}} \quad \text{.....(6)}$$

where q_e is the adsorbate amount adsorbed at equilibrium (mg/g), C_e is the adsorbate concentration at equilibrium (mg/L), Q_{max} is the maximum adsorption capacity of the adsorbent (mg/g) and K_L is Langmuir equilibrium constant (L/mg). The Langmuir isotherm can also be explained in terms of separation factor R_L, which is given as:

$$R_L = \frac{1}{(1+K_LC_0)} \quad \text{.....(7)}$$

Where C_0 is the maximum initial concentration. From the value of R_L, it can be determined whether the isotherm is irreversible ($R_L = 0$), linear ($R_L = 1$), or unfavorable ($R_L > 1$). For an ideal reaction, the value of R_L should be – $0 < R_L < 1$.

In the case of Freundlich isotherm, the mathematical equation is expressed as follows:

$$q_e = K_F.C_e^{\frac{1}{n}} \quad \text{or} \quad \log q_e = \log K_F + \frac{1}{n}\log C_e \quad \text{.....(8)}$$

Where K_F is the Freundlich equilibrium constant [$mg.g^{-1}.(mg.L^{-1})^{-1/n}$] and n is the exponent of the Freundlich model. A high value of K_F refers to high adsorption. The value of 1/n determines whether the adsorption intensity attains a non-uniform distribution. When the value of 1/n is – $0 < 1/n < 1$, then it refers towards non-uniform distribution

CHAPTER-3

RESULTS AND DISCUSSIONS

3.1. FTIR ANALYSIS OF NANOCOMPOSITE

The Fourier transform infrared (FTIR) spectrum of the prepared graphene oxide (GO) sample illustrates various peaks indicative of the presence of oxygen within the sample. A detailed examination in **Figure 6** reveals distinct peaks at specific wavenumbers, notably at 1000 cm^{-1}, 1240 cm^{-1}, 1450 cm^{-1}, 1600 cm^{-1}, and 1750 cm^{-1}.

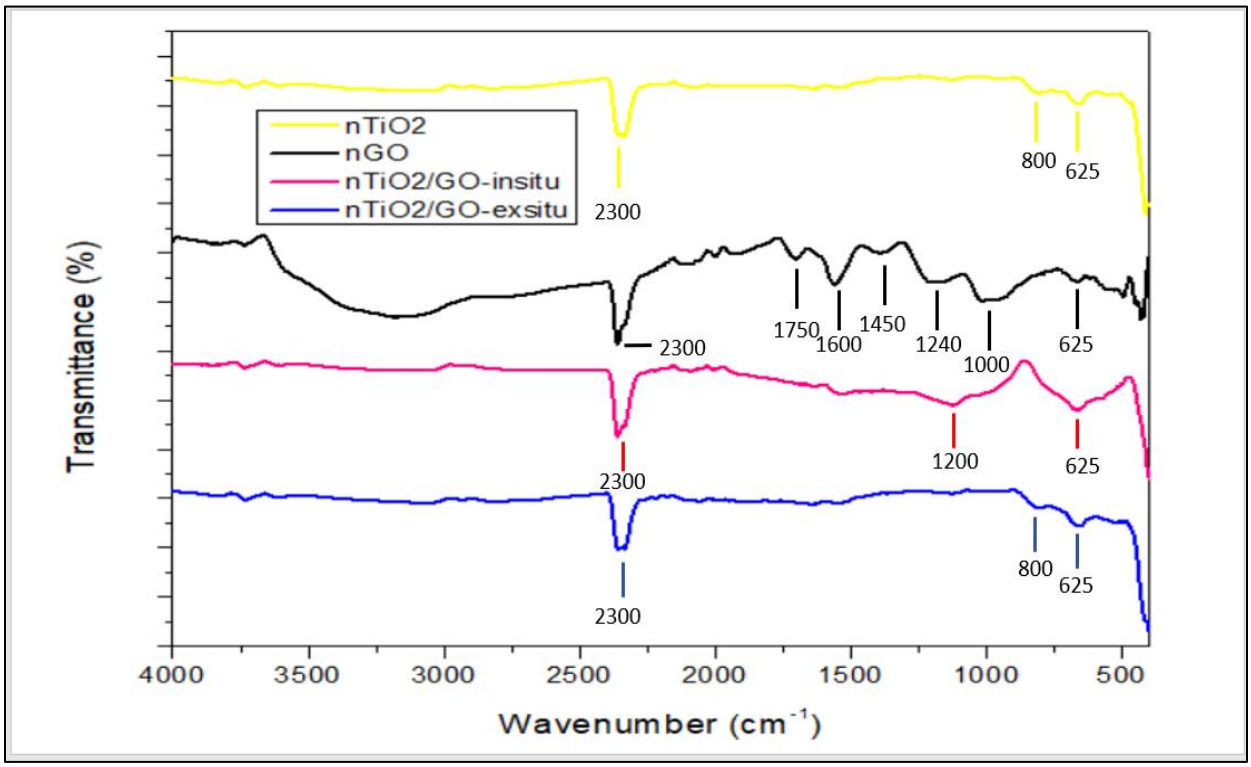


Figure 6. Plots of FTIR of nanoparticles and nanocomposites.

These peaks correspond to the characteristic functional groups present, such as the alkoxy C−O−C, epoxy C−O−C, tertiary C−OH, and carbonyl C=O groups, respectively. Furthermore, the spectral region between 3300 cm^{-1} and 3700 cm^{-1} is attributed to the O−H bond stretching vibrations originating from the hydroxyl groups in the GO structure. Additionally, the observation of a peak at 1600 cm^{-1} suggests the persistence of sp^2 bonds within the graphene oxide framework. This data from the FTIR analysis provides valuable insights into the chemical composition and structural properties of the GO sample, allowing for a comprehensive understanding of its molecular structure and functional group distribution. Furthermore, it is notable that the intensity of the bands associated with oxygen-containing bonds experienced a decrease following the partial reduction of the graphene oxide (GO) during the annealing process of the samples. This effect is clearly

illustrated in Figure 6, where the absence of new bands is evident in the doped TiO_2 nanoparticles. The reason for this absence lies in the fact that no covalent bonds were established within the composites. Specifically, in the case of GO/TiO_2, the in-situ analysis reveals shifts in the bands from 1240 to 1200 cm^{-1}, while the ex-situ examination displays similarities to TiO_2 peaks at 800 cm-1, signifying the presence of characteristic C-H bending functional groups. Moreover, the peak observed at 2300 cm^{-1} indicates O=C=O stretching, which can be attributed to the presence of atmospheric carbon dioxide within the instrument as a result of adsorption. These spectroscopic findings suggest a nuanced understanding of the chemical interactions occurring within the GO/TiO_2 composites and provide valuable insights into the structural modifications induced by annealing processes.

3.2. SEM ANALYSIS OF MEMBRANE

In the provided **Figure 7** the scanning electron microscopy (SEM) images showcase the surface characteristics of both the PVDF-PEG and GO/TiO_2 PVDF-PEG membrane/thin film, together with detailed cross-sectional views captured at various magnification levels. Upon close inspection and cross-section perspectives of the PVDF-PEG membrane/thin film, distinct features are revealed. Particularly, in the presence of PEG within the PVDF-PEG membrane, the formation of light-dark porous holes is observed, attributed to the pore-forming properties of PEG. This results in a heterogeneous surface structure, where certain areas exhibit a flat surface profile alongside a cross-sectional structure characterized by a crinkled and spongy appearance due to the addition of PEG. Moving on to the TiO_2/GO PVDF-PEG composite membrane/thin film, further analysis of the varied zooming surfaces and cross-sectional views unveils unique characteristics. Notably, the incorporation of GO introduces lamellar structures, each displaying differential light-dark patterns, suggestive of variations in transmittance and indicating that the GO layer is not uniformly structured at the nanoscale. Furthermore, the modification of the GO/TiO_2 nanocomposite with PEG leads to improved dispersibility and reduced agglomeration, as evidenced by the presence of grey and white particles within the polymer matrix, formed due to TiO_2 aggregation during the casting process. The synergy between TiO_2 and GO enhances the membrane/thin film's hydrophilicity and facilitates the dispersion of GO within the polymer matrix through van der Waals forces.

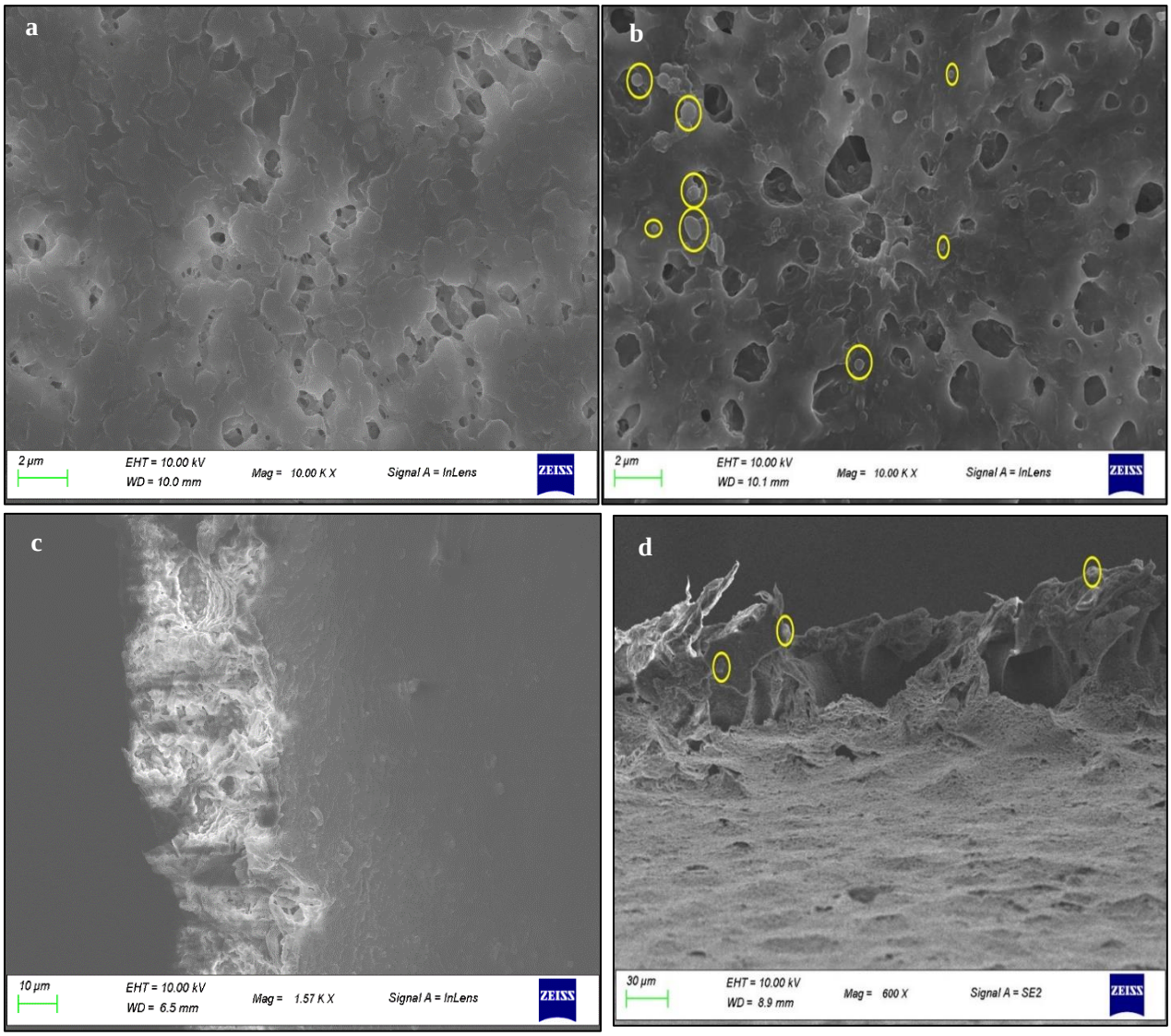


Figure 7.SEM image of PVDF-PEG(b-top view,d-cross-sectional view) and GO/TiO_2-PVDF-PEG(b-top view,d-cross-sectional view) membrane/thin film.

An intriguing observation lies in the finger-like pore structure apparent in the cross-sectional image of the GO/TiO_2 PVDF-PEG (figure-d) composite membrane, a consequence of the synergistic interactions between the GO-TiO_2 nanocomposite and the PVDF matrix facilitated by hydrogen bonding. The enhanced cross-linking within the composite membrane leads to a denser pore structure, consequently improving water flux and selectivity. With an increasing quantity of GO/TiO_2 nanocomposite within the PVDF-PEG membrane, a notable transition is observed wherein the top surface layer becomes more porous and less compact, while the bottom layer densifies, indicating the structural modifications induced by the composite material at different concentrations.

3.3. XRD ANALYSIS OF NANOCOMPOSITE

The 2θ peak shift observed at 9.03° in GO suggests complete oxidation of graphite to GO. This shift signifies a transformation due to chemical oxidation. Additionally, the interlayer distance in GO has been notably increased to 0.9794 nm, as evidenced by a d-spacing of 0.9794 nm with a FWHM of 0.6298. This expansion in interlayer space can be attributed to the incorporation of oxide functional groups, including epoxy, hydroxyl, carbonyl, and carboxyl groups, into the carbon basal plane during the oxidation process. This intercalation of functional groups has led to a noticeable increase in the separation between successive carbon layers, underlining the structural changes brought about by the oxidation of graphite into GO. The observed changes in peak shift and interlayer distance provide insights into the chemical modifications and structural alterations occurring on the nanoscale level in GO[62].

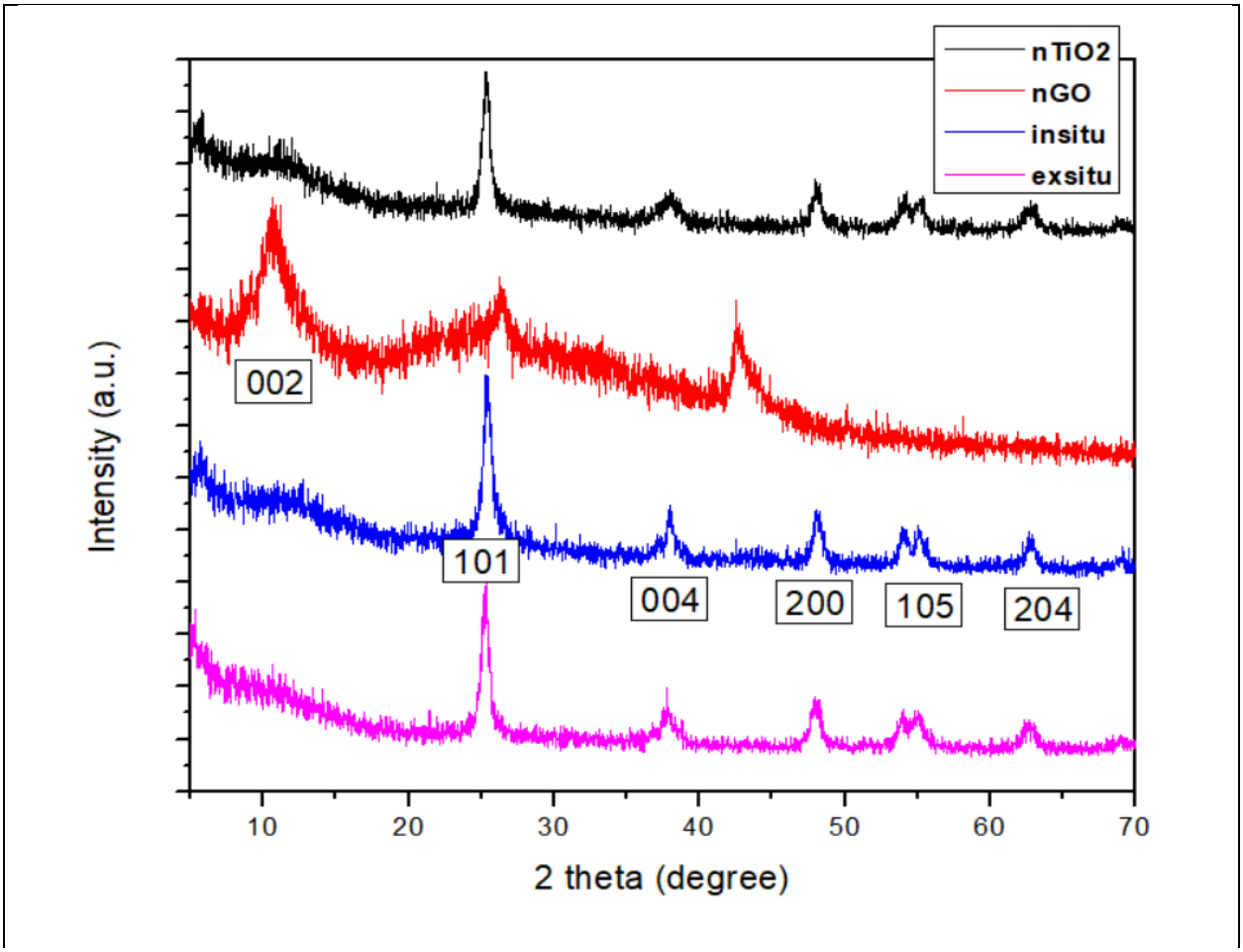


Figure 8. Plots of XRD of nanoparticles and nanocomposites.

In the XRD investigation, the TiO_2/GO combination was thoroughly examined, and the results have been displayed in **Figure 8,** It is worth noting that when observing the TiO_2/GO material, no distinctive diffraction peaks linked to layered GO were observed. This absence of noticeable layer-stacking regularity post-reduction by cations suggests a transformation in the structural configuration. Interestingly, the recorded XRD peaks predominantly align with specific crystallographic planes such as (101), (004), (200), and (105 and 204) of the anatase phase. These findings provide valuable insights into the orientation and arrangement of the integrated components. Moreover, the broad diffraction peaks observed for the TiO_2/GO composite have shed light on the particle size characteristics of the TiO_2 nanoparticles present within the material. The diminutive nature of these particles, as indicated by the diffraction patterns, signifies a finely dispersed distribution of TiO_2 within the matrix. Overall, the XRD analysis not only confirms the successful synthesis of the TiO_2/GO composite but also provides crucial information regarding its structural properties and elemental composition. The detailed examination of the diffraction patterns has allowed for a deeper understanding of the material's crystal structure and particle size distribution, emphasizing the significance of these results in the context of material science research[63].

3.4. PL ANALYSIS OF NANOCOMPOSITE

Photoluminescence (PL) spectroscopy is a powerful technique that provides crucial insights into the effectiveness of capturing and recombining charge carriers within semiconductor particles. The figure illustrates the PL assessment of the TiO_2/GO-nanocomposite (In-situ), revealing distinct peaks at 369.5 nm, indicative of a band gap (3.3559 eV) transition emission aligning with the incident light energy equal to the band gap energy of anatase. Furthermore, the additional peaks observed in the wavelength range of 440 to 525 nm are associated with exciton PL, primarily stemming from surface defects and oxygen vacancies. Notably, the PL intensity of the TiO_2/GO-nanocomposite (In-situ) markedly contrasts with that of TiO_2 nanoparticles, underscoring a reduced recombination rate for electrons and holes upon exposure to light. This diminished recombination rate can be attributed to the electrons' migration from the valence band to the conduction band and their subsequent transfer to GO sheets due to the remarkable electronic conductivity of the latter, thereby impeding prompt recombination of charge carriers. In contrast, the PL behavior of the TiO_2/GO-nanocomposite (ex-situ) closely resembles that of TiO_2 nanoparticles, suggesting inadequate bonding between GO and TiO_2 in the ex-situ case.

Consequently, it can be inferred that the In-situ configuration demonstrates both enhanced adsorption capabilities and photocatalytic activity compared to the ex-situ counterpart.

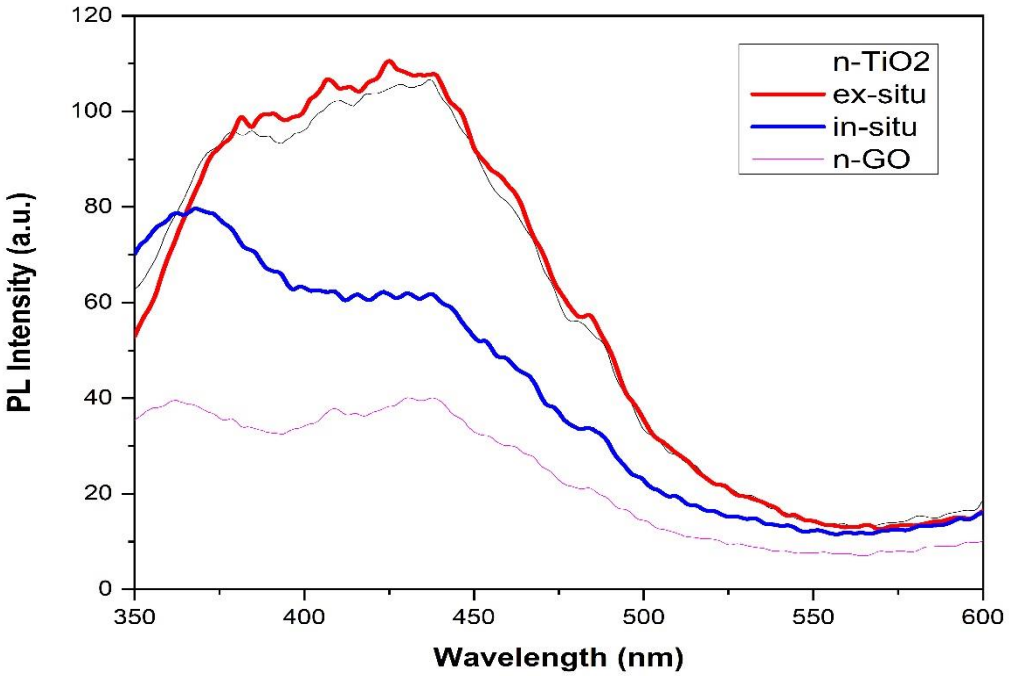


Figure 9. Plots of PL of nanoparticles and nanocomposites

3.5.BATCH EXPERIMENT OF MEMBRANE

3.5.1.The Point Of Zero Charge

100 mL Erlenmeyer flasks as part of the standard experimental setup. Each of these solutions was initially adjusted to specific pH values (pHi= 2, 4, 6, 8, 10) to create a diverse set for testing purposes. Subsequently, a precisely measured amount of $4cm^2$ of GO/TiO_2 membrane/thin film, equivalent to 0.0615gm, was placed into each solution. The next step was agitation for 24 hours at room temperature (30°C) to ensure that equilibrium pH was reached within the system. After the 24-hour agitation period, the final pH (pH_f) of each solution was meticulously measured using a pH meter, providing the essential data for further calculations. By calculating the difference between pH_f and pH_i for each solution, a meaningful dataset was obtained and graphically interpreted to gain insights into the behavior of the system. Notably, the conclusive outcome of

this rigorous methodology was the fixed value of pH 7.48, a crucial result that formed the foundation of the subsequent study's conclusions.

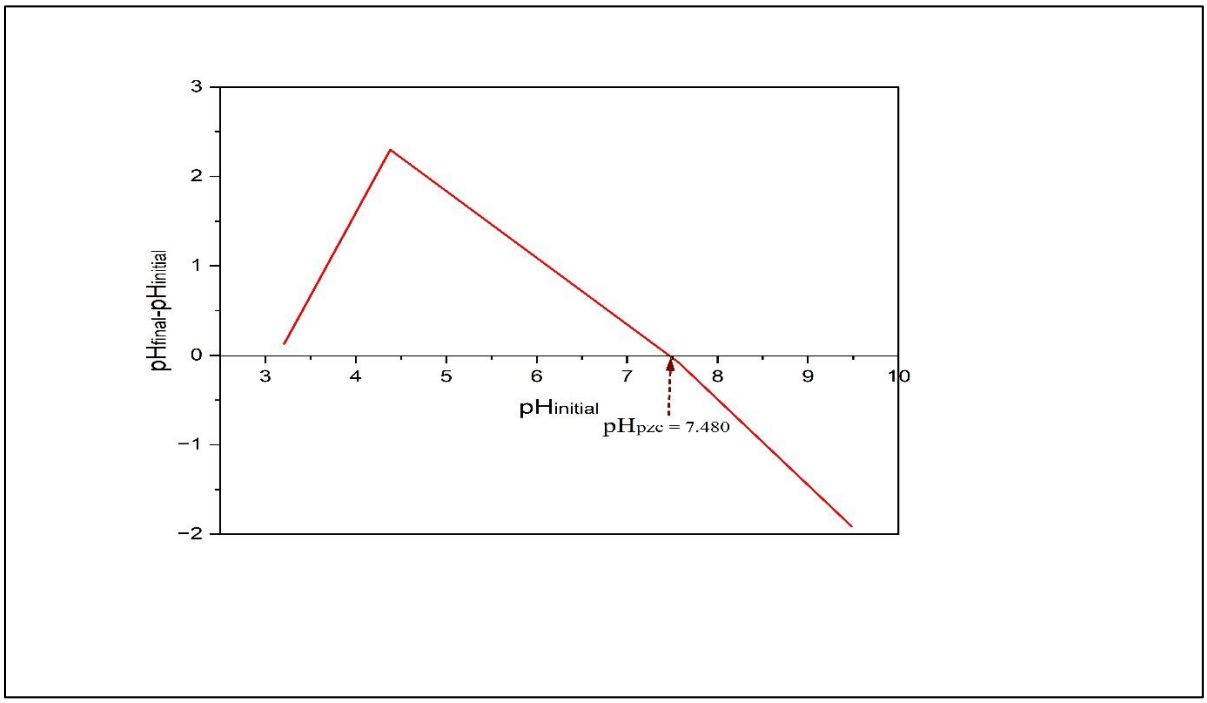


Figure 10. Plot of determination of the point of zero charge (PZC)

3.5.2. UV-Vis Spectrophotometer Analysis

For the purpose of establishing a relationship between absorbance and concentration using UV-Vis Spectroscopy, a series of solutions were meticulously prepared. These included the standard solutions of Methylene Blue (MB), Safranin O (SO), a mix of MB and SO, and potassium

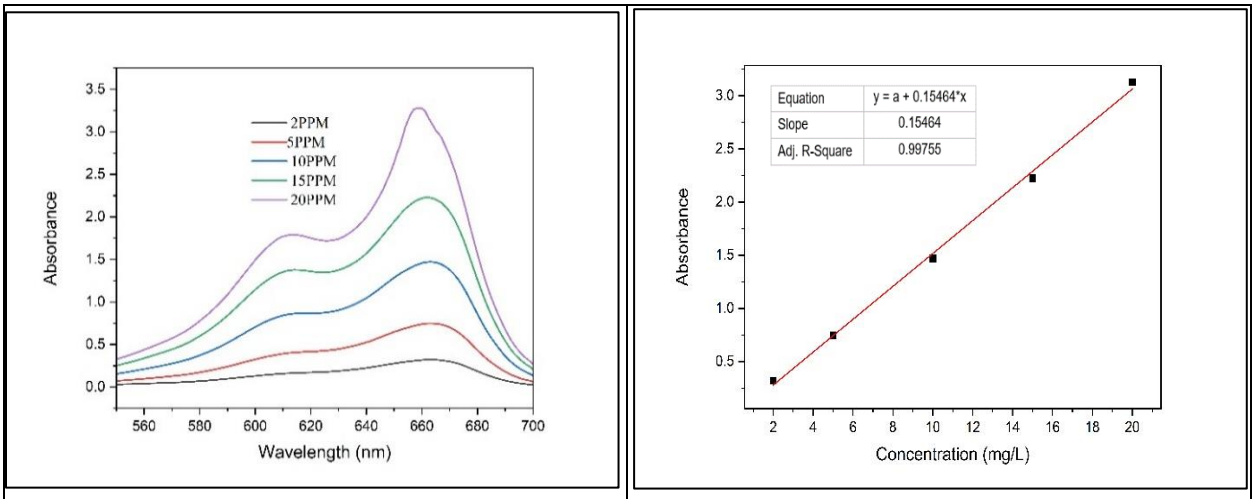


Figure 11a. Plots of the Calibration curve of MB dye

dichromate ($K_2Cr_2O_7$) at concentrations of 5 mg/L, 10 mg/L, 12.5 mg/L, 15 mg/L, 20 mg/L, 25 mg/L, and 30 mg/L. Initially, the solutions were rigorously analyzed across specific wavelength

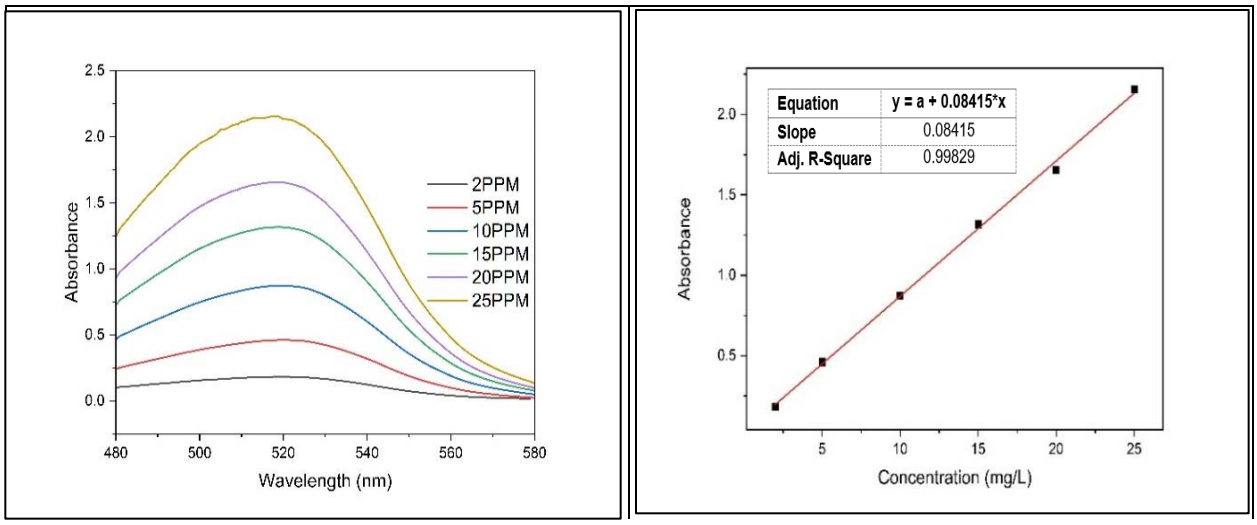


Figure 11b. Plots of the Calibration curve of SO dye.

ranges: 550-700 nm for MB, 480-580 nm for SO, 480-700 nm for the mixed solution of MB and SO, and 200-400 nm for $K_2Cr_2O_7$. Within these ranges, distinctive peak absorbance values were observed at 664 nm for MB, 521 nm for SO, and 350 nm for $K_2Cr_2O_7$.

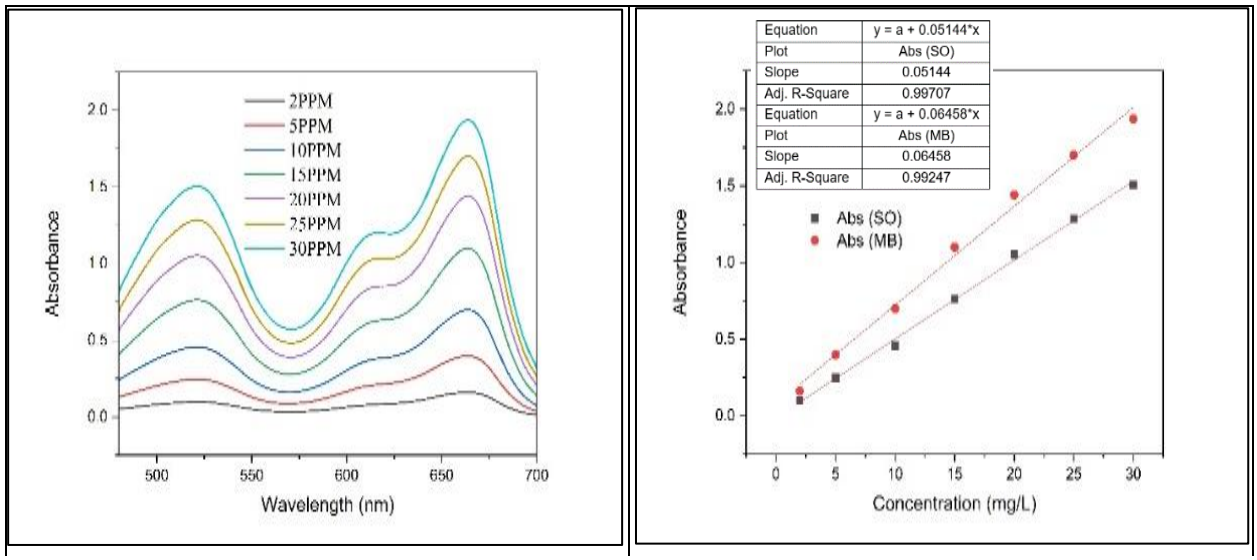


Figure 11C. Plots of the Calibration curve of Mixed dye (MB+SO)

This comprehensive experimental approach allowed for the precise characterization of the absorbance-concentration relationship, contributing valuable insights to the field of analytical chemistry through the utilization of advanced spectroscopic techniques.

Absorbance = Concentration x **Slope**

The slope of MB is 0.15464, The slope of SO is 0.08415, The slope of Mixed dye (for MB 0.06458 and SO 0.05144), and The slope of $K_2Cr_2O_7$ is 0.02626.

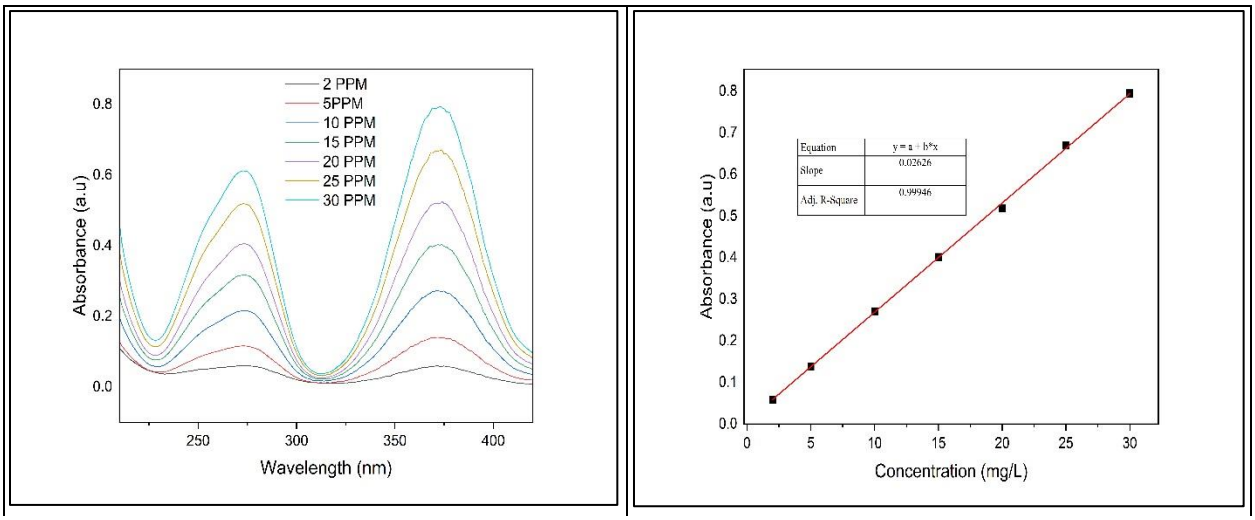


Figure 11d. Plots of the Calibration curve of $K_2Cr_2O_7$.

3.5.3. Photocatalytic Activity

The initial phase of the experiment revolves around subjecting a one-hour film sample to a dark medium, carefully designed to enhance the adsorption process effectively. Placing the sample in this environment sets the stage for subsequent evaluations by optimizing its interaction with external elements, thereby laying a strong foundation for comprehensive analysis. Transitioning the sample into a UV medium marks a pivotal juncture in the experimentation, as it undergoes controlled UV degradation that enables researchers to observe and document the film's evolving characteristics and behavior under ultraviolet influence. This systematic sequence of processes not only allows for an in-depth examination of the film's attributes but also provides valuable insights into its response to varying environmental conditions. By evaluating the percentages of adsorption based on a specific equation, a quantitative measure is introduced, adding a structured approach to the assessment methodology. Overall, this meticulous methodology ensures a rigorous assessment of the film's resilience and performance metrics, shedding light on its potential applications and stability factors. The deliberate steps taken from the dark to UV medium underscore the significance of methodical experimentation in drawing meaningful conclusions about the film's properties, thus contributing to a comprehensive understanding of its behavior in diverse settings. The percentages of adsorption capacity(up to 60 min) of the membrane were evaluated using Equation 2.

The percentage MB dye adsorption capacity of the membrane is 54.47%.

The percentage SO dye adsorption capacity of the membrane is 39.538%.

The percentage of $K_2Cr_2O_7$ adsorption capacity of the membrane is 21.664%.

The percentage of Mixed (MB+SO) dye adsorption capacity of the membrane is 47.152% for MB and 49.78% for SO.

The synthesized GO/TiO_2-PEG-PVDF film underwent an assessment of its photocatalytic activity, which involved evaluating its effectiveness in degrading MB dye, SO dye, a mixture of both dyes (MB&SO), and reduction of potassium dichromate ($K_2Cr_2O_7$) upon exposure to UV irradiation. For this evaluation, the photodegradation efficiency of the mentioned substances was closely examined to determine the film's performance under controlled conditions. The efficiency

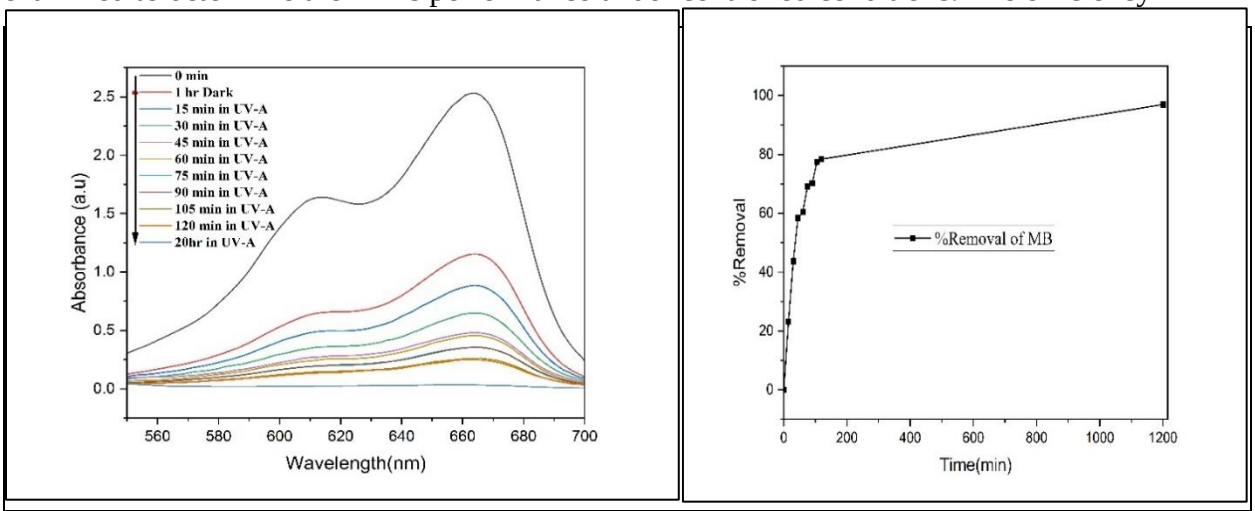


Figure 12a. Plots of %Removal with time of MB dye in UV-A medium.

of the film was meticulously analyzed by studying its degradative capacity towards the target substances over specific irradiation periods. By subjecting the film to varying durations of UV exposure, its photodegradation capabilities towards MB dye, SO dye, the mixture of both dyes (MB&SO), and potassium dichromate ($K_2Cr_2O_7$) were thoroughly investigated. These tests were

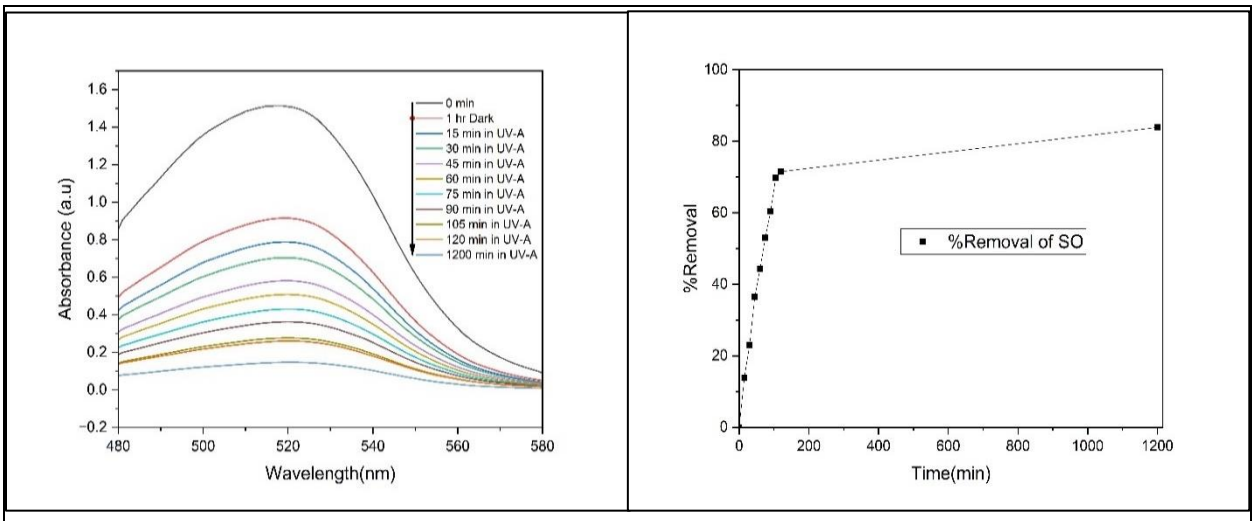


Figure 12b. Plots of %Removal with time of SO dye in UV-A medium.

conducted to measure the film's effectiveness in breaking down the target substances under consistent UV irradiation levels and exposure times. Through a systematic assessment based on irradiation durations, the film's degradation efficiency towards the specified substances was quantified and compared, providing valuable insights into its photocatalytic performance for potential applications in environmental remediation and wastewater treatment. The results are shown in **Figure 12-a,b,c,d** which displays the UV−visible spectra of MB dye, SO dye, a mixture of both dyes (MB&SO), and potassium dichromate ($K_2Cr_2O_7$) recorded at different time intervals during the photodegradation experiments. The total percentages of photodegradation were evaluated using Equation 3

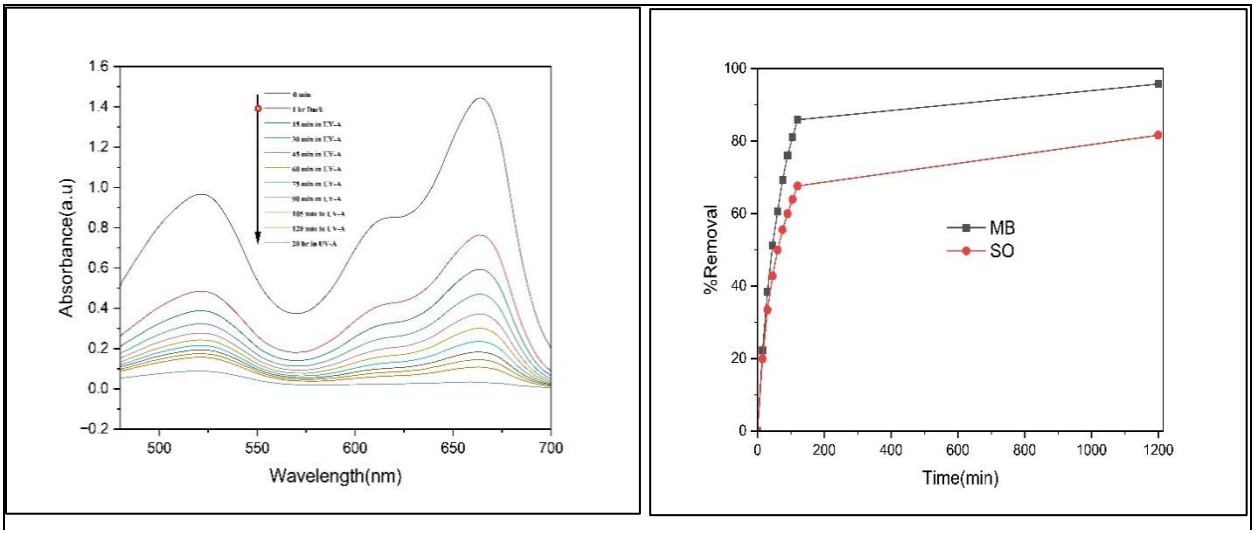


Figure 12c. Plots of %Removal with time of Mixed (MB+SO) dye in UV-A medium.

The degradation percentage of the methylene blue (MB), safranin O (SO), a mixture of MB and SO, as well as potassium dichromate ($K_2Cr_2O_7$), was assessed after exposing them to GO−TiO2 (containing 7 wt % GO) under UV irradiation for a duration of 120 minutes (about 2 hours). The results showed significant degradation levels, with percentage values of 78.388% for MB, 71.52% for SO, (85.872% for the MB and 67.638 for SO) mixture, and 95.09% for $K_2Cr_2O_7$ **(Figure 12-a,b,c,d).**

One of the most crucial factors influencing the degradation process of dyes through photocatalysis is the pH 7 for dye and pH~2 for $K_2Cr_2O_7$ level, which plays a significant role in altering the surface charge characteristics of the photocatalyst and the behavior of ionic species within the solution. According to a study by Soltani et al., during an equilibrium state in the absence of light for 60 minutes, it was noted that increasing the pH to a level of 6.0

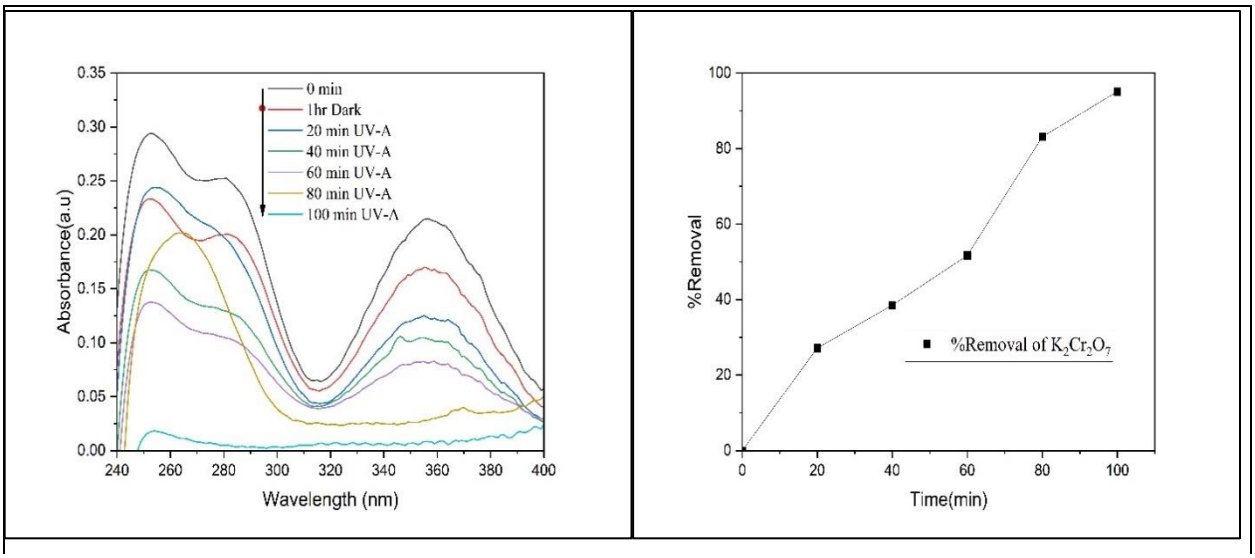


Figure 12d. Plots of %Removal with time of $K_2Cr_2O_7$ in UV-A medium.

resulted in negligible adsorption occurring. Notably, in environments with a basic pH, the photocatalytic catalyst displayed no significant absorption capacity when no light was present. However, intriguing findings emerged when examining the removal efficiency of Methylene Blue (MB) under sunlight exposure, showing that the degradation of the dye was observable in both acidic and basic solutions. This observation underscores the complex interplay between pH levels, the characteristics of the photocatalyst, and the efficiency of the degradation process when exposed to sunlight. The varying behaviors highlighted suggest that pH adjustments can directly impact the adsorption and subsequent degradation of dye molecules, with sunlight further enhancing the

efficiency of the photocatalytic process across different pH environments. In conclusion, understanding the intricate relationship between pH, catalyst properties, and light exposure is essential for optimizing the photocatalytic degradation of dyes in a diverse range of environmental conditions [33].

3.5.4. Degradation kinetics

The photodegradation reactions for dye follow pseudo-first-order kinetics. This means that the rate at which the dye degrades is directly proportional to its concentration. In order to determine the rate constants (k) of the catalytic reactions, we use an equation that involves the time of UV irradiation (t) as a key parameter, shown in **Figure 13 a,b,c.**

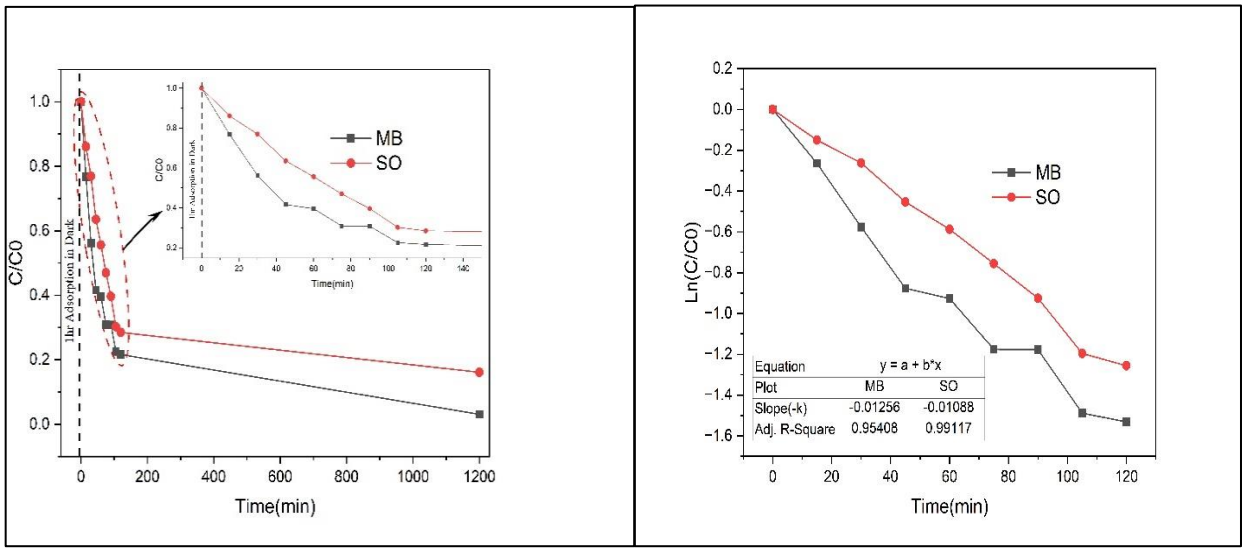


Figure 13a.Kinetic plots of the photodegradation reaction of MB and SO dye in the presence of GO/TiO_2 nanocomposites.

The degradation of MB by the $GO{-}TiO_2$ photocatalyst exhibited a defined kinetic pattern, characterized by a rate constant of 0.01256 min^{-1}. Similarly, the degradation of SO by the same photocatalyst revealed kinetics governed by a rate constant of 0.01086 min^{-1}. Interestingly, when

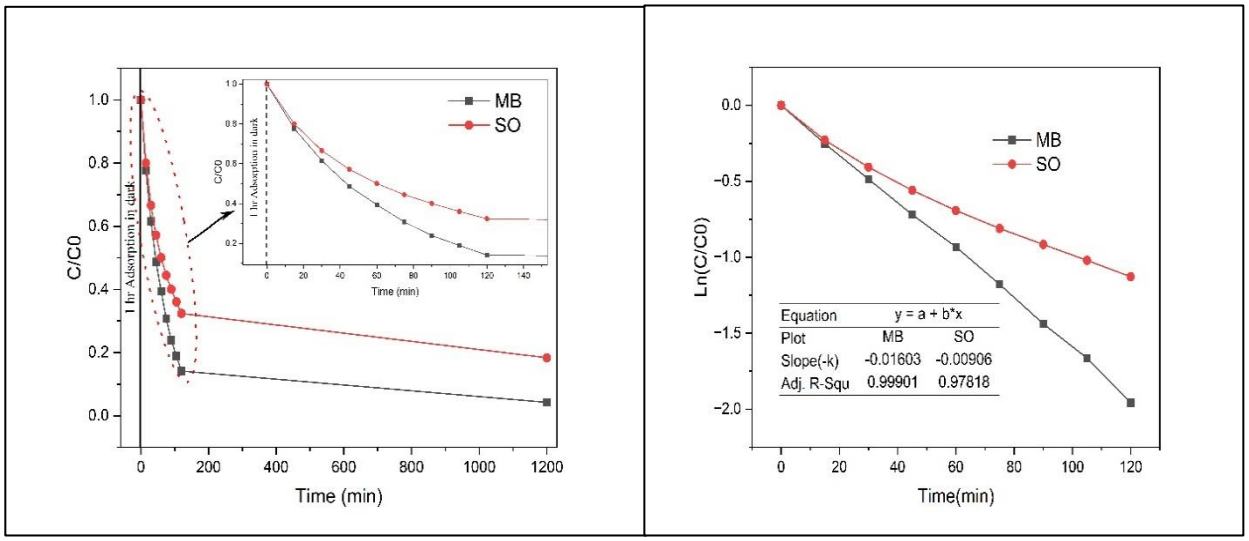


Figure 13b. Kinetic plots of the photodegradation reaction of Mixed (MB+SO) dye in the presence of GO/TiO_2 nanocomposites.

a mixture of MB and SO was subjected to the GO−TiO_2 photocatalyst, distinct degradation kinetics were observed, with rate constants of 0.01603 min^{-1} for MB and 0.00906 min^{-1} for SO. Furthermore, the application of the GO−TiO_2 photocatalyst to the degradation of Potassium Dichromate ($K_2Cr_2O_7$) resulted in kinetics characterized by a rate constant of 0.01176 min^{-1}. These findings highlight the varying efficacy of the GO−TiO_2 photocatalyst in degrading different compounds, emphasizing the role of specific rate constants in governing degradation processes and underscoring the importance of understanding the unique kinetics associated with each compound's degradation when utilizing photocatalytic systems.

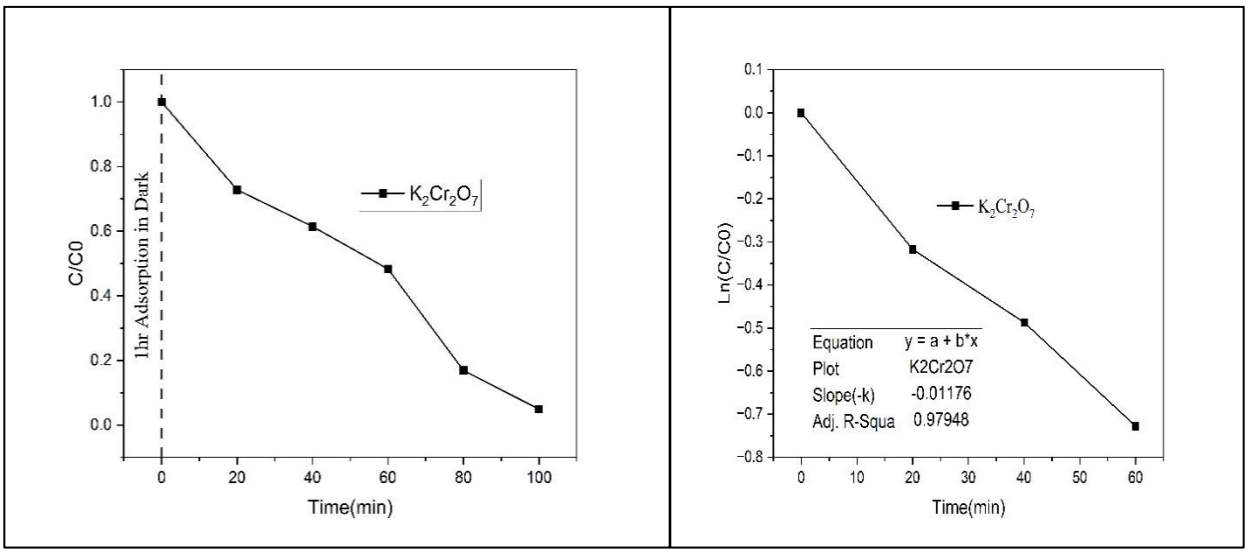


Figure 13c. Kinetic plots of the photodegradation reaction of $K_2Cr_2O_7$ in the presence of GO/TiO_2 nanocomposites.

3.5.5. Adsorption Isotherm Studies

The results derived from analyzing the Langmuir and Freundlich isotherm models can be conveniently organized and compared in the concise format presented in **Table 1**. It is important to note, as discussed in Chapter 2, that the separation factor R_L should ideally fall within the range of 0 to 1 for an optimal reaction system. Through the utilization of the Langmuir equilibrium constant K_L, which is determined from the analysis of the Langmuir isotherm, the calculated value of R_L demonstrates excellent alignment within this desirable range. Moreover, the maximum adsorption capacity (Qmax) extrapolated from the Langmuir isotherm model is notably specified as 6.18544 mg/g, with a remarkable R^2 value of 0.99772, underpinning the reliability of the obtained data. The quantifiable Freundlich equilibrium constant K_F showcases a notable indication of robust adsorption capacity, further reinforced by the calculated 1/n value of 0.74825. This value of 1/n, falling between 0 and 1, signifies that the adsorption mechanism exhibits a more heterogeneous distribution, as evidenced by the calculated R^2 value of 0.98977. This comprehensive analysis underscores the superiority of the Langmuir isotherm model over the Freundlich counterpart, as the closer proximity of the R^2 value to 1 in the Langmuir model outlines its greater suitability and reliability within the context of this study, shown in **Figures 14 &15**.

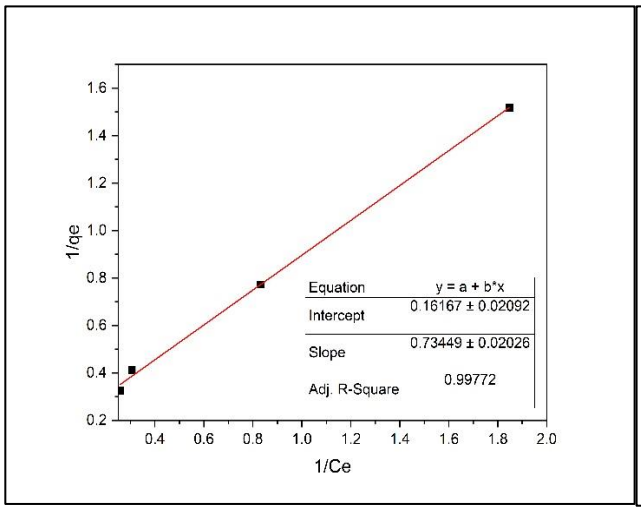


Figure 14. Isotherm study graphs for Langmuir Isotherm.

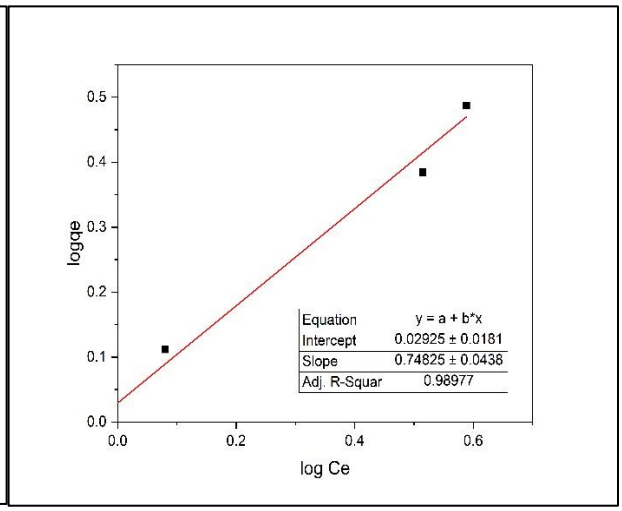


Figure 15. Isotherm study graphs for Freundlich isotherm.

Langmuir Isotherm	
Equation	$\frac{1}{q_e} = \frac{1}{K_L Q_{max}} \frac{1}{C_e} + \frac{1}{Q_{max}}$
Q_{max} (mg/g)	6.18544
K_L (L/mg)	0.220112
R_L	0.185108
R^2	0.99772
Freundlich Isotherm	
Equation	$\log q_e = \log K_F + \frac{1}{n} \log C_e$
K_F (mg/g (mg/L)$^{-1/n}$)	1.0697
1/n	0.74825
n	1.33645
R^2	0.98977

Table 1 Isotherm analysis

3.6. TENSILE STRENGTH ANALYSIS OF MEMBRANE

The polymer matrix was pivotal in the performance of the PVDF-PEG membrane/thin film, which attained a notable tensile strength of 0.842846 MPa along with a breaking strain of 10.120%. In contrast, the GO/TiO_2 PVDF-PEG composite exhibited superior elastic properties, boasting a tensile strength of 6.2201 MPa and an elongation at breakage of 9.352%, also enhancing toughness713.24%, as shown in **Table 2**. The addition of GO/TiO_2 proved to be advantageous as it significantly increased the tensile strength of the composite membrane/thin film while maintaining similar elongation properties, as shown in **Figure 16.** This enhancement in mechanical stretchability positions the composite membrane as a promising candidate for a wide range of applications, underlining its potential for various practical uses where improved performance and durability are essential. The composite membrane's ability to combine enhanced tensile strength

with consistent elongation at breakage marks a significant advancement in materials science, suggesting a bright future for this innovative technology in addressing diverse challenges across different industries.

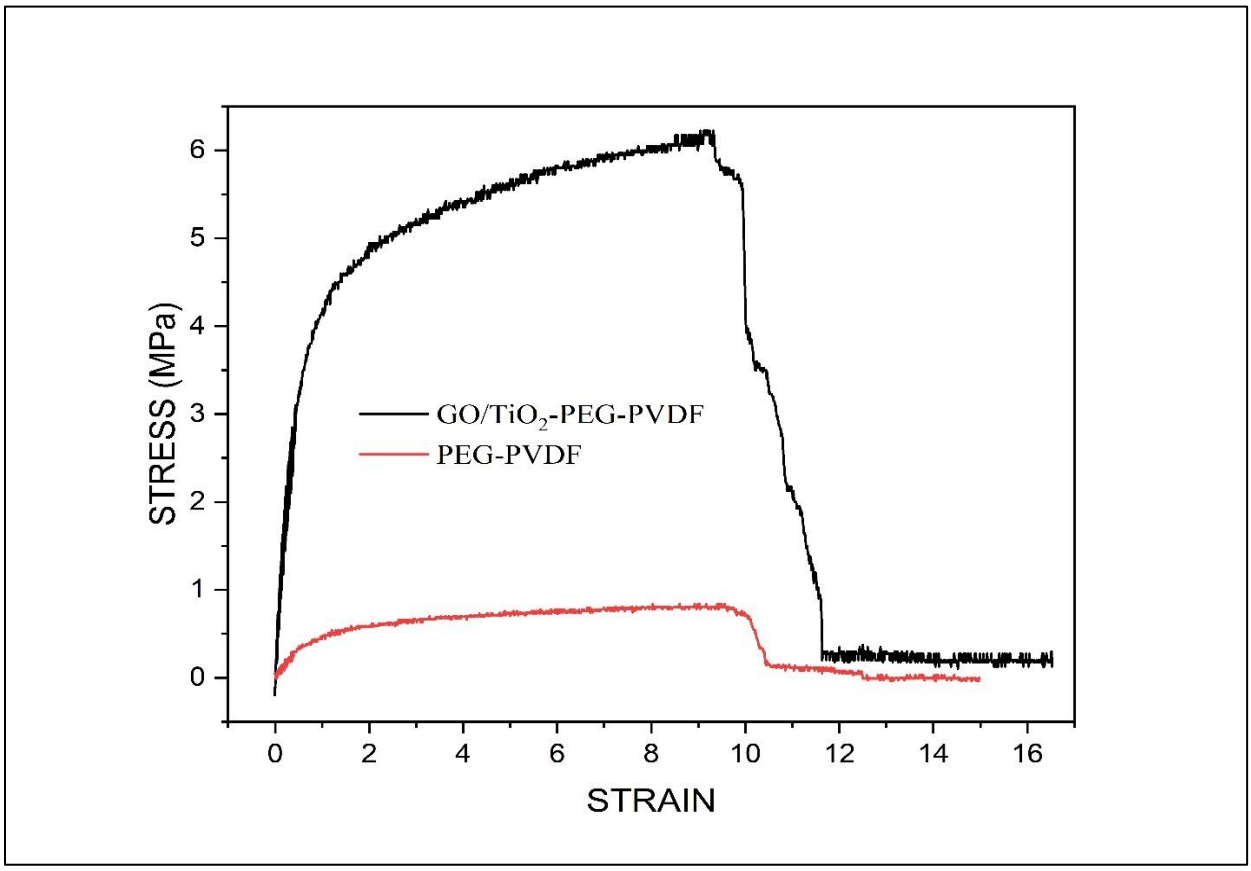


Figure16. Plots of the Tensile Strength

Description	Values(GO/TiO2-PVDF-PEG)	Values(PVDF-PEG)
Max Stress (MPa)	6.22006067	0.842846
Elongation at Break	9.3192617	9.56299319
Elastic Modulus(MPa)	4.3615	0.119
Yield Strength(MPa)	6.0400437	0.63919146
Strain at yield	9.3520119	10.1205852
Strain at failure	11.6381744	10.446683
Toughness	57.83741	7.11193
Resilience	2.6193	0.4691

Table 2. Data of Tensile Strength analysis

3.7. SWELLING EXPERIMENT OF MEMBRANE

In the laboratory, when measuring the swelling property of a polymer membrane, it is essential to have a comprehensive understanding of how the membrane/thin film reacts to various solvents. Among the methods that can be utilized for this purpose, the Gravimetric Method stands out. This method involves immersing a dry membrane/thin film (initially weighing 40.9 mg and covering an area of 4 cm^2) into different types of solvents for stability assessment over time. Equation 1 is then applied to calculate the percentage swelling at various time intervals. Throughout the study, a range of solvents such as NMP, DMF, Distilled Water, Salinity Water (15000ppm), 2-propanol, Ethanol, and Acetone were employed. An interesting observation was made with DMF and NMP, as these solvents led to the dissolution of the membrane/thin film within just 20 minutes. In contrast, when immersed in Distilled Water, the membrane exhibited a significant swelling percentage of 207.09% over 3 hours. Similarly, in Salinity Water, the swelling percentage reached 147.68% over the same time period, while in 2-propanol, it was 152.57%, in Ethanol, it was 134.47%, and in Acetone, a remarkable 368.22%. By graphing %swelling against time, a clear visualization of the data was achieved, providing valuable insights into the behavior of the polymer membrane/thin film in response to different solvents, as shown in **Figure 17.**

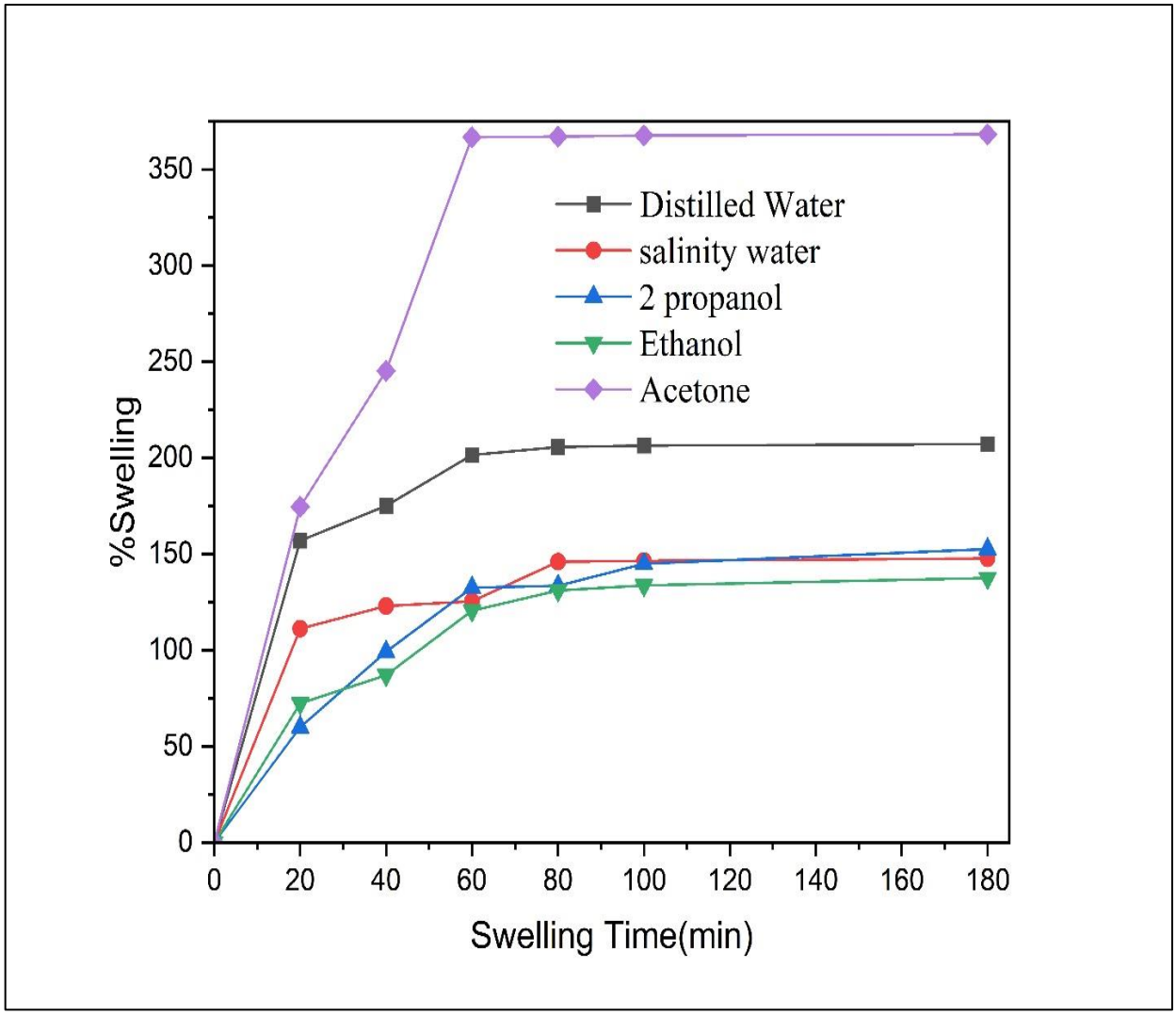


Figure 17. Plots of %Swelling of the membrane/thin film in different solvents with time

3.8.REGENERATION STUDY OF MEMBRANE

In this detailed study, a comprehensive range of desorption solutions was harnessed to facilitate membrane/thin film regeneration. These solutions included pure hydrochloric acid (HCl), unsullied ethanol, an amalgamation of equal proportions of HCl and ethanol, a mixture consisting of equal volumes of sodium hydroxide (NaOH) and ethanol, and a concoction blending equal volumes of acetic acid and ethanol. Notably, after subjecting the membrane to four thorough wash cycles utilizing a combination of equal parts HCl and ethanol, an impressive 73% of dye removal was achieved without inducing any damage to the membrane/thin film structure. Contrastingly,

the efficacy of the other desorption solutions was less impressive, failing to surpass the 60% mark for dye removal. particularly concerning was the impact of solutions like the mixture of equal volumes of sodium hydroxide (NaOH) and ethanol, which not only fell short in terms of dye removal but also had detrimental effects on the overall longevity of the membrane. A visual representation of the % removal against the number of cycles, as depicted in Figure 18, offers a clear visualization of the comparative performance of the various desorption solutions employed in this rigorous experimentation.

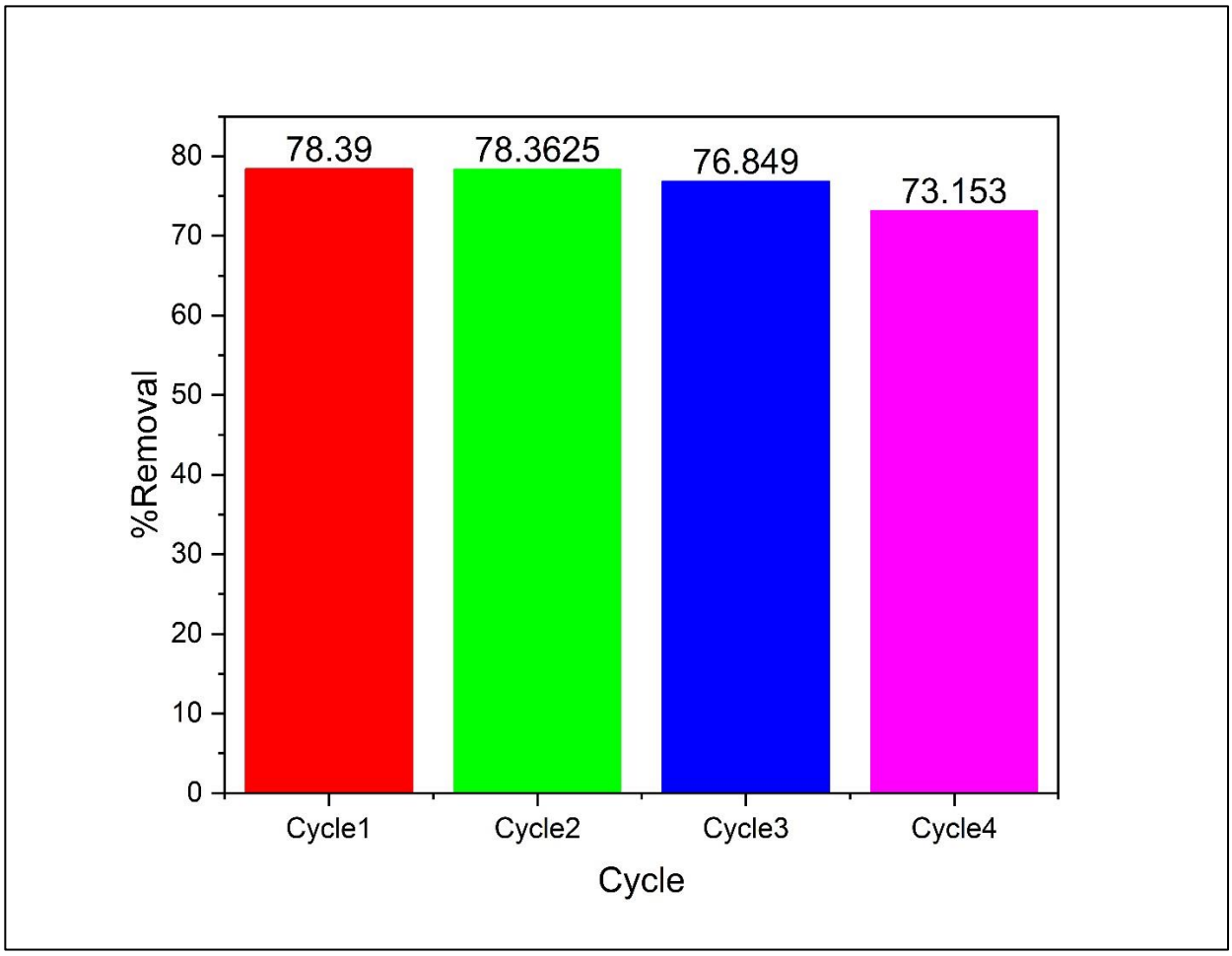


Figure 18 Regeneration of membrane/thin film bar graphs

CHAPTER -4

CONCLUSION

4.1.CONCLUSION

The inclusion of GO/TiO_2 composite nanomaterials in the fabrication of GO/TiO_2 -PVDF hybrid membrane/thin film proved to be a significant advancement in membrane technology. It was found that the addition of these composites did not alter the crystal structure of the PVDF polymer. This was attributed to the superior particle distribution of GO /TiO_2 compared to PVDF. The enhanced distribution of particles led to an improvement in the surface hydrophilicity, mean pore size, and overall porosity of the PVDF hybrid membranes. Consequently, this enhancement played a pivotal role in boosting the anti-fouling properties of the GO/TiO_2-PVDF hybrid membrane/thin film to a significant extent.

In the membrane preparation process, the pivotal role of PEG grafted on GO/TiO_2 as a pore-forming additive was observed. This addition resulted in an increase in the pore structure on the membrane's surface due to the heightened polarity of TiO_2–O. The introduction of PEG-modified GO/TiO_2 further enhanced the surface hydrophilicity of the PVDF hybrid membranes, setting them apart from membrane/thin film containing unmodified GO/TiO_2 composites. Notably, the incorporation of PEG modification had the most pronounced impact on boosting the surface hydrophilicity of the membrane/thin film.

Therefore, it can be concluded that the PVDF hybrid membrane/thin film containing GO/TiO_2 -PEG demonstrated superior performance in terms of surface hydrophilicity and membrane efficiency. The remarkable removal percentages of key contaminants such as MB, SO, and $K_2Cr_2O_7$ at the 120-minute mark, along with the increase in stress reaching 6.22006067MPa and toughness increases 713.24%, further underscored the effectiveness of the GO/TiO_2 -PVDF-PEG hybrid membranes in water treatment applications.

The term “membrane/thin film” has been used since all the expectations were carried out in batch mode. It is worthwhile to mention here that as per our expectation, the same set of experiments would also yield successful results if a synthesized fabrication is applied to a continuous mode of experiment for the removal of contaminants from wastewater streams.

References

[1] N. A. A. Qasem, R. H. Mohammed, and D. U. Lawal, "Removal of heavy metal ions from wastewater: a comprehensive and critical review," *npj Clean Water*, vol. 4, no. 1. Nature Research, Dec. 01, 2021. doi: 10.1038/s41545-021-00127-0.

[2] M. M. Pendergast and E. M. V. Hoek, "A review of water treatment membrane nanotechnologies," *Energy and Environmental Science*, vol. 4, no. 6. pp. 1946–1971, Jun. 2011. doi: 10.1039/c0ee00541j.

[3] P. S. Goh, T. Matsuura, A. F. Ismail, and N. Hilal, "Recent trends in membranes and membrane processes for desalination," *Desalination*, vol. 391, pp. 43–60, Aug. 2016, doi: 10.1016/j.desal.2015.12.016.

[4] R. K. Joshi, S. Alwarappan, M. Yoshimura, V. Sahajwalla, and Y. Nishina, "Graphene oxide: The new membrane material," *Applied Materials Today*, vol. 1, no. 1. Elsevier Ltd, pp. 1–12, 2015. doi: 10.1016/j.apmt.2015.06.002.

[5] W. Zhang, Z. Shi, F. Zhang, X. Liu, J. Jin, and L. Jiang, "Superhydrophobic and superoleophilic PVDF membranes for effective separation of water-in-oil emulsions with high flux," *Advanced Materials*, vol. 25, no. 14, pp. 2071–2076, Apr. 2013, doi: 10.1002/adma.201204520.

[6] X. Huang *et al.*, "Treatment of oily waste water by PVP grafted PVDF ultrafiltration membranes," *Chemical Engineering Journal*, vol. 273, pp. 421–429, Aug. 2015, doi: 10.1016/j.cej.2015.03.086.

[7] X. Lin, M. Yang, H. Jeong, M. Chang, and J. Hong, "Durable superhydrophilic coatings formed for anti-biofouling and oil-water separation," *J Memb Sci*, vol. 506, pp. 22–30, May 2016, doi: 10.1016/j.memsci.2016.01.035.

[8] L. Bai, Y. Liu, A. Ding, N. Ren, G. Li, and H. Liang, "Surface coating of UF membranes to improve antifouling properties: A comparison study between cellulose nanocrystals (CNCs) and cellulose nanofibrils (CNFs)," *Chemosphere*, vol. 217, pp. 76–84, Feb. 2019, doi: 10.1016/j.chemosphere.2018.10.219.

[9] F. Liu, N. A. Hashim, Y. Liu, M. R. M. Abed, and K. Li, "Progress in the production and modification of PVDF membranes," *Journal of Membrane Science*, vol. 375, no. 1–2. pp. 1–27, Jun. 15, 2011. doi: 10.1016/j.memsci.2011.03.014.

[10] M. Safarpour, A. Khataee, and V. Vatanpour, "Preparation of a novel polyvinylidene fluoride (PVDF) ultrafiltration membrane modified with reduced graphene oxide/titanium dioxide (TiO2) nanocomposite with enhanced hydrophilicity and antifouling properties," *Ind Eng Chem Res*, vol. 53, no. 34, pp. 13370–13382, Aug. 2014, doi: 10.1021/ie502407g.

[11] Y. H. Tan, P. S. Goh, A. F. Ismail, B. C. Ng, and G. S. Lai, "Decolourization of aerobically treated palm oil mill effluent (AT-POME) using polyvinylidene fluoride (PVDF) ultrafiltration membrane incorporated with coupled zinc-iron oxide nanoparticles," *Chemical Engineering Journal*, vol. 308, pp. 359–369, Jan. 2017, doi: 10.1016/j.cej.2016.09.092.

[12] H. Wang *et al.*, "Enhancement of hydrophilicity and the resistance for irreversible fouling of polysulfone (PSF) membrane immobilized with graphene oxide (GO) through chloromethylated and quaternized reaction," *Chemical Engineering Journal*, vol. 334, pp. 2068–2078, Feb. 2018, doi: 10.1016/j.cej.2017.11.135.

[13] C. Ma *et al.*, "Graphene oxide-polyethylene glycol incorporated PVDF nanocomposite ultrafiltration membrane with enhanced hydrophilicity, permeability, and antifouling performance," *Chemosphere*, vol. 253, Aug. 2020, doi: 10.1016/j.chemosphere.2020.126649.

[14] S. Ghosh and K. Chatterjee, "Poly(Ethylene glycol) functionalized graphene oxide in tissue engineering: A review on recent advances," *International Journal of Nanomedicine*, vol. 15. Dove Medical Press Ltd., pp. 5991–6006, 2020. doi: 10.2147/IJN.S249717.

[15] B. Liu, B. Chen, and B. Zhang, "Oily Wastewater Treatment by Nano-TiO2-Induced Photocatalysis: Seeking more efficient and feasible solutions.," *IEEE Nanotechnol Mag*, vol. 11, no. 3, pp. 4–15, Sep. 2017, doi: 10.1109/MNANO.2017.2708818.

[16] J. A. Byrne *et al.*, "A review of heterogeneous photocatalysis for water and surface disinfection," *Molecules*, vol. 20, no. 4, pp. 5574–5615, Apr. 2015, doi: 10.3390/molecules20045574.

[17] A. O. Ibhadon and P. Fitzpatrick, "Heterogeneous photocatalysis: Recent advances and applications," *Catalysts*, vol. 3, no. 1. Multidisciplinary Digital Publishing Institute (MDPI), pp. 189–218, Mar. 04, 2013. doi: 10.3390/catal3010189.

[18] C. Uboldi *et al.*, "Role of the crystalline form of titanium dioxide nanoparticles: Rutile, and not anatase, induces toxic effects in Balb/3T3 mouse fibroblasts," *Toxicology in Vitro*, vol. 31, pp. 137–145, Mar. 2016, doi: 10.1016/j.tiv.2015.11.005.

[19] S. M. Hussain, K. L. Hess, J. M. Gearhart, K. T. Geiss, and J. J. Schlager, "In vitro toxicity of nanoparticles in BRL 3A rat liver cells," in *Toxicology in Vitro*, Oct. 2005, pp. 975–983. doi: 10.1016/j.tiv.2005.06.034.

[20] H. Hidaka,',', Y. Suzuki,' Kayo Nohara,' Satoshi Horikoshi,', Y. Hisamatsu, E. Pelizzettl, and N. Serpone4, "Photocatalyzed Degradation of Polymers in Aqueous Semiconductor Suspensions. 1. Photooxidation of Solid Particles of Polyvinylchloride."

[21] R. Molinari *et al.*, “Study on a photocatalytic membrane reactor for water purification,” 2000.

[22] L. guang Wu, X. yang Zhang, T. Wang, C. hui Du, and C. hong Yang, “Enhanced performance of polyvinylidene fluoride ultrafiltration membranes by incorporating TiO2/graphene oxide,” *Chemical Engineering Research and Design*, vol. 141, pp. 492–501, Jan. 2019, doi: 10.1016/j.cherd.2018.11.025.

[23] N. A. F. Al-Rawashdeh, O. Allabadi, and M. T. Aljarrah, “Photocatalytic activity of graphene oxide/zinc oxide nanocomposites with embedded metal nanoparticles for the degradation of organic dyes,” *ACS Omega*, vol. 5, no. 43, pp. 28046–28055, Nov. 2020, doi: 10.1021/acsomega.0c03608.

[24] E. Dadvar, R. R. Kalantary, H. Ahmad Panahi, and M. Peyravi, “Efficiency of Polymeric Membrane Graphene Oxide-TiO2 for Removal of Azo Dye,” *Journal of Chemistry*, vol. 2017. Hindawi Limited, 2017. doi: 10.1155/2017/6217987.

[25] J. Prakash, “Mechanistic Insights into Graphene Oxide Driven Photocatalysis as Co-Catalyst and Sole Catalyst in Degradation of Organic Dye Pollutants,” *Photochem*, vol. 2, no. 3. Multidisciplinary Digital Publishing Institute (MDPI), pp. 651–671, Sep. 01, 2022. doi: 10.3390/photochem2030043.

[26] F. Dai *et al.*, “Preparation and Characterization of Reduced Graphene Oxide /TiO2 Blended Polyphenylene sulfone Antifouling Composite Membrane With Improved Photocatalytic Degradation Performance,” *Front Chem*, vol. 9, Oct. 2021, doi: 10.3389/fchem.2021.753741.

[27] B. Mustafa *et al.*, “Next-generation graphene oxide additives composite membranes for emerging organic micropollutants removal: Separation, adsorption and degradation,” *Chemosphere*, vol. 308, Dec. 2022, doi: 10.1016/j.chemosphere.2022.136333.

[28] M. Golmohammadi *et al.*, “Photocatalytic nanocomposite membranes for environmental remediation,” *Nanotechnology*, vol. 33, no. 46, Nov. 2022, doi: 10.1088/1361-6528/ac8682.

[29] J. Romão, D. Barata, P. Habibovic, G. Mul, and J. Baltrusaitis, “High throughput analysis of photocatalytic water purification,” *Anal Chem*, vol. 86, no. 15, pp. 7612–7617, Aug. 2014, doi: 10.1021/ac501426f.

[30] R. Thiruvenkatachari, S. Vigneswaran, and I. S. Moon, “A review on UV/TiO 2 photocatalytic oxidation process,” 2008.

[31] M. C. Rosu *et al.*, “Azo dyes degradation using TiO2-Pt/graphene oxide and TiO2-Pt/reduced graphene oxide photocatalysts under UV and natural sunlight irradiation,” *Solid State Sci*, vol. 70, pp. 13–20, Aug. 2017, doi: 10.1016/j.solidstatesciences.2017.05.013.

[32] L. Zhang *et al.*, "Significantly enhanced photocatalytic activities and charge separation mechanism of Pd-decorated ZnO-graphene oxide nanocomposites," *ACS Appl Mater Interfaces*, vol. 6, no. 5, pp. 3623–3629, Mar. 2014, doi: 10.1021/am405872r.

[33] T. Soltani and M. H. Entezari, "Photolysis and photocatalysis of methylene blue by ferrite bismuth nanoparticles under sunlight irradiation," *J Mol Catal A Chem*, vol. 377, pp. 197–203, 2013, doi: 10.1016/j.molcata.2013.05.004.

[34] J. Prakash, S. Sun, H. C. Swart, and R. K. Gupta, "Noble metals-TiO2 nanocomposites: From fundamental mechanisms to photocatalysis, surface enhanced Raman scattering and antibacterial applications," *Applied Materials Today*, vol. 11. Elsevier Ltd, pp. 82–135, Jun. 01, 2018. doi: 10.1016/j.apmt.2018.02.002.

[35] N. Singh, J. Prakash, and R. K. Gupta, "Design and engineering of high-performance photocatalytic systems based on metal oxide-graphene-noble metal nanocomposites," *Molecular Systems Design and Engineering*, vol. 2, no. 4. Royal Society of Chemistry, pp. 422–439, 2017. doi: 10.1039/c7me00038c.

[36] N. Singh, J. Prakash, M. Misra, A. Sharma, and R. K. Gupta, "Dual Functional Ta-Doped Electrospun TiO2 Nanofibers with Enhanced Photocatalysis and SERS Detection for Organic Compounds," *ACS Appl Mater Interfaces*, vol. 9, no. 34, pp. 28495–28507, Aug. 2017, doi: 10.1021/acsami.7b07571.

[37] S. Kumar and A. Kumar, "Chemically derived luminescent graphene oxide nanosheets and its sunlight driven photocatalytic activity against methylene blue dye," *Opt Mater (Amst)*, vol. 62, pp. 320–327, Dec. 2016, doi: 10.1016/j.optmat.2016.10.014.

[38] K. Govindan *et al.*, "Effect of peroxomonosulfate, peroxodisulfate and hydrogen peroxide on graphene oxide photocatalytic performances in methyl orange dye degradation," *Chemosphere*, vol. 237, Dec. 2019, doi: 10.1016/j.chemosphere.2019.124479.

[39] T. Gupta, Samriti, J. Cho, and J. Prakash, "Hydrothermal synthesis of TiO2 nanorods: formation chemistry, growth mechanism, and tailoring of surface properties for photocatalytic activities," *Materials Today Chemistry*, vol. 20. Elsevier Ltd, Jun. 01, 2021. doi: 10.1016/j.mtchem.2021.100428.

[40] S. Víctor-Román *et al.*, "Controlling the surface chemistry of graphene oxide: Key towards efficient ZnO-GO photocatalysts," *Catal Today*, vol. 357, pp. 350–360, Nov. 2020, doi: 10.1016/j.cattod.2019.05.049.

[41] T. D. Nguyen-Phan *et al.*, "The role of graphene oxide content on the adsorption-enhanced photocatalysis of titanium dioxide/graphene oxide composites," *Chemical Engineering Journal*, vol. 170, no. 1, pp. 226–232, May 2011, doi: 10.1016/j.cej.2011.03.060.

[42] W. Iqbal, B. Tian, M. Anpo, and J. Zhang, "Single-step solvothermal synthesis of mesoporous anatase TiO2-reduced graphene oxide nanocomposites for the abatement of organic pollutants," *Research on Chemical Intermediates*, vol. 43, no. 9, pp. 5187–5201, Sep. 2017, doi: 10.1007/s11164-017-3049-6.

[43] Y. Haldorai, B. K. Kim, Y. L. Jo, and J. J. Shim, "Ag@graphene oxide nanocomposite as an efficient visible-light plasmonic photocatalyst for the degradation of organic pollutants: A facile green synthetic approach," *Mater Chem Phys*, vol. 143, no. 3, pp. 1452–1461, Feb. 2014, doi: 10.1016/j.matchemphys.2013.11.065.

[44] K. Krishnamoorthy, R. Mohan, and S. J. Kim, "Graphene oxide as a photocatalytic material," *Appl Phys Lett*, vol. 98, no. 24, Jun. 2011, doi: 10.1063/1.3599453.

[45] M. Singh, N. K. Bajaj, A. Bhardwaj, P. Singh, P. Kumar, and J. Sharma, "Study of photocatalytic and antibacterial activities of graphene oxide nanosheets," *Adv Compos Hybrid Mater*, vol. 1, no. 4, pp. 759–765, Dec. 2018, doi: 10.1007/s42114-018-0056-z.

[46] Y. Chen, L. Wang, H. Sun, D. Zhang, Y. Zhao, and L. Chen, "Self-assembling TiO2 on aminated graphene based on adsorption and catalysis to treat organic dyes," *Appl Surf Sci*, vol. 539, Feb. 2021, doi: 10.1016/j.apsusc.2020.147889.

[47] Y. Gao, M. Hu, and B. Mi, "Membrane surface modification with TiO2-graphene oxide for enhanced photocatalytic performance," *J Memb Sci*, vol. 455, pp. 349–356, Apr. 2014, doi: 10.1016/j.memsci.2014.01.011.

[48] G. Riegel and J. R. Bolton, "Photocatalytic Efficiency Variability in Ti02 Particles," 1995.

[49] Y. M. Hunge *et al.*, "Enhanced photocatalytic performance of ultrasound treated GO/TiO2 composite for photocatalytic degradation of salicylic acid under sunlight illumination," *Ultrason Sonochem*, vol. 61, Mar. 2020, doi: 10.1016/j.ultsonch.2019.104849.

[50] C. H. Nguyen, M. L. Tran, T. T. Van Tran, and R. S. Juang, "Enhanced removal of various dyes from aqueous solutions by UV and simulated solar photocatalysis over TiO2/ZnO/rGO composites," *Sep Purif Technol*, vol. 232, Feb. 2020, doi: 10.1016/j.seppur.2019.115962.

[51] M. Romay, N. Diban, M. J. Rivero, A. Urtiaga, and I. Ortiz, "Critical issues and guidelines to improve the performance of photocatalytic polymeric membranes," *Catalysts*, vol. 10, no. 5. MDPI, May 01, 2020. doi: 10.3390/catal10050570.

[52] D. T. Tran, J. Mendret, J. P. Méricq, C. Faur, and S. Brosillon, "Study of permeate flux behavior during photo-filtration using photocatalytic composite membranes," *Chemical Engineering and Processing - Process Intensification*, vol. 148, Feb. 2020, doi: 10.1016/j.cep.2019.107781.

[53] X. Chang, Z. Wang, S. Quan, Y. Xu, Z. Jiang, and L. Shao, "Exploring the synergetic effects of graphene oxide (GO) and polyvinylpyrrodione (PVP) on poly(vinylylidenefluoride) (PVDF) ultrafiltration Membrane performance," *Appl Surf Sci*, vol. 316, no. 1, pp. 537–548, 2014, doi: 10.1016/j.apsusc.2014.07.202.

[54] V. Bhatia, A. Dhir, and A. K. Ray, "Photocatalytic degradation of atenolol with graphene oxide/zinc oxide composite: Optimization of process parameters using statistical method," *J Photochem Photobiol A Chem*, vol. 409, Mar. 2021, doi: 10.1016/j.jphotochem.2021.113136.

[55] A. Ajmal, I. Majeed, R. N. Malik, H. Idriss, and M. A. Nadeem, "Principles and mechanisms of photocatalytic dye degradation on TiO 2 based photocatalysts: A comparative overview," *RSC Advances*, vol. 4, no. 70. Royal Society of Chemistry, pp. 37003–37026, 2014. doi: 10.1039/c4ra06658h.

[56] S. O. Cigdem, "Adsorption and desorption kinetics behaviour of methylene blue onto activated carbon," *Physicochemical Problems of Mineral Processing*, vol. 48, no. 2, pp. 441–454, 2012, doi: 10.5277/ppmp120210.

[57] M. V. Kangralkar, V. A. Kangralkar, and J. Manjanna, "Adsorption of Cr (VI) and photodegradation of rhodamine b, rose bengal and methyl red on Cu2O nanoparticles," *Environ Nanotechnol Monit Manag*, vol. 15, May 2021, doi: 10.1016/j.enmm.2020.100417.

[58] S. A. Mousa, H. Abdallah, S. S. Ibrahim, and S. A. Khairy, "Enhanced photocatalytic properties of graphene oxide/polyvinylchloride membranes by incorporation with green prepared SnO2 and TiO2 nanocomposite for water treatment," *Appl Phys A Mater Sci Process*, vol. 129, no. 12, Dec. 2023, doi: 10.1007/s00339-023-07117-8.

[59] N. F. Bunkin *et al.*, "Dynamics of polymer membrane swelling in aqueous suspension of amino-acids with different isotopic composition; photoluminescence spectroscopy experiments," *Polymers (Basel)*, vol. 13, no. 16, Aug. 2021, doi: 10.3390/polym13162635.

[60] L. Zheng, Y. Su, L. Wang, and Z. Jiang, "Adsorption and recovery of methylene blue from aqueous solution through ultrafiltration technique," *Sep Purif Technol*, vol. 68, no. 2, pp. 244–249, Aug. 2009, doi: 10.1016/j.seppur.2009.05.010.

[61] Ş. Ş. Türkyılmaz, N. Güy, and M. Özacar, "Photocatalytic efficiencies of Ni, Mn, Fe and Ag doped ZnO nanostructures synthesized by hydrothermal method: The synergistic/antagonistic effect between ZnO

and metals," *J Photochem Photobiol A Chem*, vol. 341, pp. 39–50, May 2017, doi: 10.1016/j.jphotochem.2017.03.027.

[62] N. M. S. Hidayah *et al.*, "Comparison on graphite, graphene oxide and reduced graphene oxide: Synthesis and characterization," in *AIP Conference Proceedings*, American Institute of Physics Inc., Oct. 2017. doi: 10.1063/1.5005764.

[63] S. Sagadevan, K. Pal, P. Koteeswari, and A. Subashini, "Synthesis and characterization of TiO2/graphene oxide nanocomposite," *Journal of Materials Science: Materials in Electronics*, vol. 28, no. 11, pp. 7892–7898, Jun. 2017, doi: 10.1007/s10854-017-6488-3.